Colloquium: Quantum limits to the energy resolution of magnetic field sensors

Morgan W. Mitchell

ICFO—Institut de Ciencies Fotoniques, The Barcelona Institute of Science and Technology, 08860 Castelldefels, Barcelona, Spain
and ICREA—Institució Catalana de Recerca i Estudis Avançats, 08010 Barcelona, Spain

Silvana Palacios Alvarez

ICFO—Institut de Ciencies Fotoniques, The Barcelona Institute of Science and Technology, 08860 Castelldefels, Barcelona, Spain

(published 28 April 2020)

The energy resolution per bandwidth E_R is a figure of merit that combines the field resolution, bandwidth or duration of the measurement, and size of the sensed region. Several different dc magnetometer technologies approach $E_R = \hbar$, while to date none have surpassed this level. This suggests a technology-spanning quantum limit, a suggestion that is strengthened by model-based calculations for nitrogen-vacancy centers in diamond, for superconducting quantum interference device sensors, and for some optically pumped alkali-vapor magnetometers, all of which predict a quantum limit close to $E_R = \hbar$. This Colloquium reviews what is known about energy resolution limits, with the aim of understanding when and how E_R is limited by quantum effects. A survey of reported sensitivity versus size of the sensed region for more than 20 magnetometer technologies is included, the known model-based quantum limits are reviewed, and possible sources for a technology-spanning limit are critically assessed, including zero-point fluctuations, magnetic self-interaction, and quantum speed limits. Finally, sensing approaches are described that appear to be unconstrained by any of the known limits, thus making them candidates to surpass $E_R = \hbar$.

DOI: 10.1103/RevModPhys.92.021001

CONTENTS

I. INTRODUCTION

Low-frequency magnetic fields are ubiquitous and provide important information in applications ranging from nanotechnology (Ariyaratne *et al.*, 2018) to brain studies (Boto *et al.*, 2017) to space science (Arridge *et al.*, 2016). A plethora of sensing scenarios, and the availability of many physical systems with strong magnetic response, have led to many distinct magnetometer technologies. Grosz, Haji-Sheikh, and Mukhopadhyay (2016) provided a recent and extensive review. It is of both fundamental and practical interest to know how well quantum physics allows such sensors to perform. At a fundamental level, prior work on quantum limits of sensing has uncovered connections to the geometry of quantum states (Braunstein and Caves, 1994), entanglement in many-body systems (Sørensen and Mølmer, 2001), quantum information processing (Giovannetti, Lloyd, and Maccone, 2006; Roy and Braunstein, 2008), and quantum nonlocality (Tura *et al.*, 2014; Schmied *et al.*, 2016). These results for the most part concern quantum estimation theory (Helstrom, 1969, 1976) applied to generalized linear interferometers (Lee, Kok, and Dowling, 2002). High-performance magnetometers, however, employ methods not easily mapped onto linear interferometry (Mitchell, 2017), and one may hope that understanding their quantum limits will yield still other fundamental insights.

In this Colloquium, we focus on energy resolution limits (ERLs), which are constraints on the energy resolution per bandwidth E_R, a figure of merit that combines field resolution, measurement duration or bandwidth, and the size of the sensed region (Robbes, 2006). E_R has units of action, with smaller values indicating a better combination of speed, size, and sensitivity. The best magnetometer technologies now reach $E_R \approx \hbar$. ERLs near this value are predicted for important magnetometry technologies, including superconducting quantum interference devices (SQUIDs) (Koch, Van Harlingen, and Clarke, 1980), optically pumped magnetometers (OPMs) (Jiménez-Martínez and Knappe, 2017), and spin-precession sensors with fixed, random spin positions, e.g., nitrogen-vacancy centers in diamond (NVDs) (Mitchell, 2020). The nature and scope of ERLs is thus also a practical question that informs efforts to improve energy resolution beyond the current state of the art.

One of the most intriguing features of ERLs is the suggestion that there may be a single, technology-spanning ERL, one that constrains any magnetic field measurement, regardless of how it is performed. This suggestion emerges most immediately from a multitechnology survey of reported sensitivities (see Fig. 2 and Table I), all of which obey $E_R \geq \hbar$, even as some come close to this level. Given that the known limits for SQUIDs, OPMs, and NVD sensors are also near this level, it is natural to ask whether these ERLs could be distinct manifestations of a single ERL. Such a limit could plausibly be imposed by general quantum limits, for example, the Margolus-Levitin bound (Margolus and Levitin, 1998), which relates the speed of evolution to the available energy, or the Bremermann-Bekenstein bound (Bekenstein, 1981b; Bremermann, 1982), which relates the entropy and thus information content of a region to its energy content and size.

The objective of this Colloquium is to bring together, and when possible to synthesize, the many dispersed insights that bear on the question of when and how quantum mechanics constrains the energy resolution of a magnetic field sensor. The text is organized as follows: In Sec. II, we describe ERLs as they appear in the scientific literature for different sensor types. In Sec. III, we discuss the physical meaning of an ERL and note its relation to independence of quantum noise sources. In Sec. V, we present model-based ERLs for SQUIDs, alkali-vapor OPMs, and color-center (e.g., NVD) sensors. In Sec. VI, we assess technology-independent quantum limits, e.g., quantum speed limits, and their potential to supply a technology-spanning ERL. In Sec. VII, we describe sensing approaches that evade the known limits and thus may have potential to surpass current state-of-the-art energy resolutions.

II. HISTORY AND ORIGINS

The ERL concept emerged from an analysis of dc SQUID sensitivity by Tesche and Clark (Tesche and Clarke, 1977; Koch, Van Harlingen, and Clarke, 1980). A SQUID is a planar field sensor based on the Josephson effect and measures the flux Φ through a loop of superconducting material; see Fig. 1. A more detailed description is given in Sec. V. Tesche and Clarke considered a lumped-circuit model of the dc SQUID dynamics to compute the equivalent flux-noise power spectral

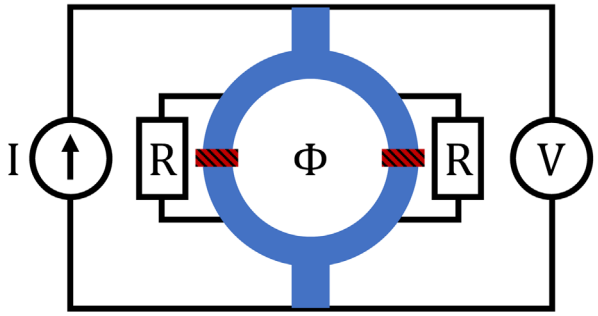

FIG. 1. Schematic diagram of a dc SQUID in constant current mode with resistively shunted Josephson junctions. A superconducting loop (thick blue) is interrupted by two Josephson junctions (dashed red). The junctions are shunted by resistances R. A constant current I feeds the SQUID, and the generated voltage V is used to infer the flux Φ threading the SQUID loop.

density $S_\Phi(\nu)$ of Φ, where ν is the linear frequency. Optimization of the SQUID parameters for best dc sensitivity, i.e., for minimum $S_\Phi(0)$, yields the bound

$$E_R^{(\text{dc SQUID})} \equiv \frac{S_\Phi(0)}{2L} \geq \hbar, \tag{1}$$

where L is the inductance of the SQUID pickup loop.[1] The name *energy resolution* was applied to $E_R = S_\Phi(0)/(2L)$ by analogy to $\Phi^2/(2L)$, the magnetostatic energy in a current loop. As should be clear from Eq. (1), E_R has units of action, not energy, and in more recent literature E_R is referred to as the *energy resolution per bandwidth*.

To compare with other kinds of sensors, it is interesting to have a purely geometric expression for this limit. To this end, we note that $\Phi = BA$, where A is the loop area, and that $L = \sqrt{A}\mu_0/\alpha$, where α is a wire geometry factor of the order of unity. We can thus reexpress the Tesche-Clarke (TC) limit as

$$E_R^{(\text{area})} \equiv \frac{S_B(0)A^{3/2}}{2\mu_0} \geq \alpha\hbar. \tag{2}$$

The use of energy resolution as a measure of sensitivity has spread to other areas, including both Bose-Einstein condensate (BEC) and hot-vapor OPMs (Vengalattore *et al.*, 2007; Dang, Maloof, and Romalis, 2010; Griffith, Knappe, and Kitching, 2010; Jiménez-Martínez and Knappe, 2017), and cross-technology reviews (Bending, 1999; Robbes, 2006; Yang *et al.*, 2017). For a planar BEC sensor, the geometrical form of the ERL, i.e., Eq. (2), has been directly used for an intertechnology comparison (Vengalattore *et al.*, 2007a). For volumetric sensors, the energy resolution has been defined with reference to $B^2V/(2\mu_0)$, the magnetostatic energy in a volume V, to give

[1]The 1977 TC publication assumed quantum noise arising from electron pair shot noise in the current across the Josephson junctions and arrived at a limit of $h/2 = \pi\hbar$. Later analyses assume quantum noise from zero-point fluctuations in resistances shunting the junctions and arrive at a limit of $\hbar$ (Koch, Van Harlingen, and Clarke, 1981; Robbes, 2006).

$$E_R^{(\mathrm{vol})} \equiv \frac{S_B(0)V}{2\mu_0}. \tag{3}$$

A first-principles study of a possible quantum bound on $E_R^{(\mathrm{vol})}$ for OPMs and a comparison against the planar ERL for SQUIDS appear to have been reported by Lee and Romalis (2008); see also Romalis *et al.* (2014).

III. NATURE AND FORM OF ENERGY RESOLUTION LIMITS

To understand the meaning of an ERL, rather than a continuous measurement, it is convenient to consider a sequence of discrete field measurements, averaged to obtain the dc field value. Consider a magnetic sensor of volume V that, after observation time T, gives a reading $B_{\mathrm{obs}} = B_{\mathrm{true}} + \delta B$, where B_{true} is the true value of the field and δB is the measurement error. We assume that through calibration of the sensor $\langle \delta B \rangle = 0$ such that B_{obs} is an unbiased estimator for B_{true}. The mean apparent magnetostatic energy in the sensor volume is

$$E_{\mathrm{obs}} = \frac{\langle B_{\mathrm{obs}}^2 \rangle V}{2\mu_0} = \frac{B_{\mathrm{true}}^2 V}{2\mu_0} + \frac{\langle \delta B^2 \rangle V}{2\mu_0} \tag{4}$$

We now consider performing such T-duration measurements as often as possible, i.e., with measurement repetition period T, and averaging them. We assume the measurement is subject to only quantum noise, all other noise sources having been reduced to negligible levels. We can then use the statistical independence of quantum noise in two ways. First, we note that $\langle \delta B^2 \rangle T = S_B(0)$, such that the second term in Eq. (4) becomes $E_R^{(\mathrm{vol})}$. We thus recognize $E_R^{(\mathrm{vol})}$ as the bias in the magnetostatic energy estimate.

Second, we note that in total acquisition time T_{acq} we can average $N_{\mathrm{rep}} \equiv T_{\mathrm{acq}}/T$ measurements to yield a variance $\langle \delta B^2 \rangle / N_{\mathrm{rep}} = \langle \delta B^2 \rangle T / T_{\mathrm{acq}}$. Given a fixed T_{acq} and a choice among measurements with different values for $\langle \delta B^2 \rangle$ and T, the measurement with the smallest $\langle \delta B^2 \rangle T$ is thus the superior measurement. If a quantum limit exists, it is because there is a limit on the product $\langle \delta B^2 \rangle T$. The same argument applies to the volume, if we imagine filling a volume with nonoverlapping sensors and averaging their readings. As a result, we expect a volumetric ERL of quantum origin to take the form

$$E_R^{(\mathrm{vol})} \equiv \frac{S_B(0)V}{2\mu_0} = \frac{\langle \delta B^2 \rangle VT}{2\mu_0} \geq \mathcal{S}, \tag{5}$$

where $\mathcal{S}$ is a constant with units of action. We use the common shorthand δB for $\langle \delta B^2 \rangle^{1/2}$ and refer to $\delta B \sqrt{T}$ as the sensitivity.

IV. SCALING OF SENSITIVITY WITH EXTENT OF THE SENSED REGION

High-sensitivity magnetometers have been demonstrated or proposed with all possible dimensionalities: pointlike, linear, planar, and volumetric. Examples of pointlike sensors are single NVDs (Fang *et al.*, 2013; Trusheim *et al.*, 2014; Lovchinsky *et al.*, 2016; Ariyaratne *et al.*, 2018) and single trapped ions (Ruster *et al.*, 2017). Linear sensors include ferromagnetic needles (Jackson Kimball, Sushkov, and Budker, 2016; Band, Avishai, and Shnirman, 2018) and some cold atomic ensembles (Sewell *et al.*, 2012; Behbood *et al.*, 2013). Planar sensors include superconducting sensors of various types (Robbes, 2006; Giazotto *et al.*, 2010; Kher *et al.*, 2013, 2016; Luomahaara *et al.*, 2014; Kher, 2017), Hall-effect sensors (Bending, 1999), and several others (Robbes, 2006; Grosz, Haji-Sheikh, and Mukhopadhyay, 2016). Volumetric sensors include OPMs (Kominis *et al.*, 2003; Dang, Maloof, and Romalis, 2010; Griffith, Knappe, and Kitching, 2010; Gawlik and Pustelny, 2017; Jiménez-Martínez and Knappe, 2017; Savukov, 2017; Weis, Bison, and Grujić, 2017), ensemble NVD sensors (Wolf *et al.*, 2015; Barry *et al.*, 2016; Jensen, Kehayias, and Budker, 2017), and others. Sensors employing trapped Bose-Einstein condensates (Wildermuth *et al.*, 2006; Vengalattore *et al.*, 2007; Yang *et al.*, 2017) or cold thermal ensembles may approximate any of these geometries, depending on the trap configuration.

Regardless of the sensor dimensionality, the field to be detected exists in three-dimensional space and, moreover, varies smoothly in that space, except near magnetic sources. Because of this, a sensor's reading is representative of the field in a three-dimensional volume, even if the sensor is of lower dimensionality. For example, we may consider a pointlike sensor embedded in a support that prevents magnetic sources to approach closer than a minimum distance l_{min}. By $\nabla \cdot \mathbf{B} = 0$, the field experienced by the sensor is equal to the average of the field inside a sphere of radius l_{min} about the sensor position. The sensor signal is the same as it would be were the sensor to uniformly sample this spherical volume. We can thus assign an effective volume $4\pi l_{\mathrm{min}}^3/3$ to the pointlike sensor. To enable a uniform comparison of different sensor types, we define $l_{\mathrm{eff}} \equiv \sqrt[3]{\mathrm{volume}}$ and $l_{\mathrm{eff}} = \sqrt{\mathrm{area}}$, respectively, for the effective linear dimensions of volumetric and planar sensors. Noting that with these definitions Eqs. (2) and (3) coincide, we can hypothesize the technology-spanning ERL

$$E_R \equiv \frac{S_B(0) l_{\mathrm{eff}}^3}{2\mu_0} = \frac{\langle \delta B^2 \rangle l_{\mathrm{eff}}^3 T}{2\mu_0} \geq \alpha \hbar, \tag{6}$$

where α is again a number of the order of unity.

In Fig. 2, we show sensitivity versus effective linear dimension for many representative publications on high-sensitivity magnetic field detection. Only measured sensitivities are included, and only when the dimensions of the sensitive region could be determined. With a few exceptions (to be discussed later), the survey is restricted to dc field sensors, which we take to include field components below 1 kHz. While most sensors operate continuously, a number of sensors in the survey operate in a pulsed mode. For example, cold atom experiments take time to accumulate atoms prior to any sensing, making their cycle time longer than the measurement time. Because we are concerned here with fundamental limits, when computing the energy resolution per bandwidth we include such delays only if they appear to be unavoidable for fundamental reasons. For example, atom-trap loading time is not included because one can imagine ways to

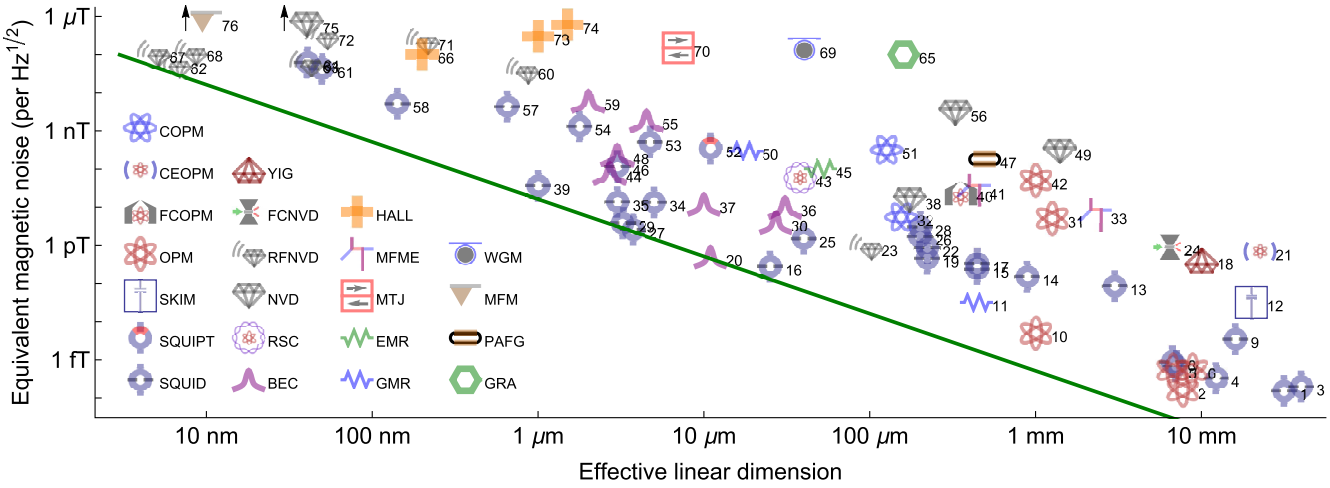

FIG. 2. Reported magnetic sensitivity $\delta B\sqrt{T}$ for different sensor technologies versus size of the sensitive region. Effective linear dimension l_{eff} indicates $\sqrt{\text{area}}$ for planar sensors and $\sqrt[3]{\text{volume}}$ for volumetric ones. For pointlike systems such as single spins, l_{eff} indicates $\sqrt[3]{\text{volume}}$ for a sphere with radius equal to the minimum source-detector distance. For work reporting sensitivity in units of magnetic dipole moment, we convert to field units using the reported sample distance. Excepting RFNVD, noise levels are the lowest reported value at frequency ≤ 1 kHz. An arrow indicates that the value is off the scale. SQUID, superconducting quantum interference device; SQUIPT, superconducting quantum interference proximity transistor; SKIM, superconducting kinetic impedance magnetometer; OPM, optically pumped magnetometer; FCOPM, OPM with flux concentrators; CEOPM, cavity-enhanced OPM; COPM, OPM with cold thermal atoms; BEC, Bose-Einstein condensate; RSC, Rydberg Schrödinger cat; NVD, nitrogen-vacancy center in diamond; RFNVD, radio-frequency NVD; FCNVD, NVD with flux concentrators; YIG, yttrium-aluminum-garnet; GMR, giant magnetoresistance; EMR, extraordinary magnetoresistance; MTJ, magnetic tunnel junction; MEMF, magnetoelectric multiferroic; HALL, Hall-effect sensor; GRA, graphene; PAFG, parallel gating fluxgate; MFM, magnetic force microscope, WGM, whispering-gallery mode magnetostrictive. Line shows $E_R \equiv \langle \delta B^2 \rangle T l_{\mathrm{eff}}^3/(2\mu_0) = \hbar$. Numeric labels refer to Table I.

deliver a new batch of atoms each time the previous batch is consumed. In contrast, delays associated with optical pumping or fluorescence detection (both of which require time for spontaneous emission) would appear to be unavoidable.

For work that reports a field-equivalent noise spectral density $S_B(\nu)$ and the dimensions of the sensitive region, no conversion of physical quantities is required. For work that reports sensitivity in units of magnetic moment μ, e.g., for magnetic microscopy applications, we convert the equivalent noise $S_\mu(\nu)$ to field units using the sample-sensor distance assuming a dipole field distribution.

As seen in Fig. 2, several different technologies come close to $E_R = \hbar$. These include micro-SQUIDs (Cromar and Carelli, 1981; Van Harlingen, Koch, and Clarke, 1982; Awschalom *et al.*, 1988; Wakai and Van Harlingen, 1988; Mück, Kycia, and Clarke, 2001), spinor Bose-Einstein condensates (Vengalattore *et al.*, 2007), and spin-exchange-relaxation-free (SERF)-regime OPMs (Dang, Maloof, and Romalis, 2010; Griffith, Knappe, and Kitching, 2010). As rf magnetometers, single nitrogen-vacancy (NV) centers in diamond (Lovchinsky *et al.*, 2016) also are close to $E_R = \hbar$.

V. KNOWN LIMITS FOR SPECIFIC TECHNOLOGIES

For three well-studied high-sensitivity magnetometer types, model-based calculations are known to lead to an ERL. We have already mentioned the TC limit for dc SQUID sensors, the origin of Eq. (1). More recent calculations for spin-precession sensors, both OPMs and NVD sensors, give rise to a limit on the volumetric energy resolution of Eq. (3). Although derived for different systems using different models, these limits appear to agree.

A. dc SQUID sensors

The dc SQUID analyzed by Tesche and Clarke (1977) consists of a loop of superconducting material interrupted by two Josephson junctions (JJs), as illustrated in Fig. 1, with a constant current bias I and resulting voltage V across the SQUID. The dynamics of the dc SQUID are, in general, complex and nonlinear, but in some regimes the SQUID provides a direct relationship between the flux Φ threading the loop and V, allowing Φ to be inferred from V, which can be measured using low-noise amplifiers. In other regimes, the flux-current relationship is hysteretic and the flux cannot simply be inferred from V. To avoid these hysteretic regimes, damping is typically introduced in the form of resistances shunting the JJs. These shunt resistances introduce both thermal noise (Johnson-Nyquist noise) and quantum noise (zero-point current fluctuations) into the SQUID dynamics. The TC analysis showed that if the resistances provide enough damping to make the flux-current relation single valued, then they also introduce enough quantum noise to impose an energy resolution limit, as in Eq. (1). The TC analysis has been extended to more detailed dc SQUID models (Koch, Van Harlingen, and Clarke, 1980; Wakai and Van Harlingen, 1988; Ryhänen *et al.*, 1989), and was reviewed by Robbes (2006). With careful construction, small dc SQUID devices have reported $S_\Phi(0)/(2L)$ as low as $2\hbar$ (Awschalom *et al.*, 1988; Wakai and Van Harlingen, 1988; Mück, Kycia, and Clarke, 2001).

TABLE I. Dimensions and field and/or flux sensitivities for the sensing results shown in Fig. 1. Values are taken directly from the cited publications when possible. In some cases, values are estimated from a graph or an image. Dots indicate values not found in the cited works.

Label	References	Type	l_1 (m)	l_2 (m)	l_3 (m)	V (m^3)	A (m^2)	$\delta\Phi\sqrt{T}$ ($T/\sqrt{Hz}$)	$\delta B\sqrt{T}$ ($Wb/\sqrt{Hz}$)	Notes
1	Schmelz *et al.* (2016)	SQUID	3.0×10^{-2}	3.4×10^{-2}	⋯	⋯	9.9×10^{-4}	⋯	1.5×10^{-16}	
2	Dang, Maloof, and Romalis (2010)	OPM	5.0×10^{-3}	5.0×10^{-3}	1.8×10^{-2}	4.5×10^{-7}	⋯	⋯	1.6×10^{-16}	
3	Storm *et al.* (2017)	SQUID	4.5×10^{-2}	4.5×10^{-2}	⋯	⋯	1.6×10^{-3}	⋯	2.0×10^{-16}	
4	Schmelz *et al.* (2011)	SQUID	1.2×10^{-2}	1.2×10^{-2}	⋯	⋯	1.5×10^{-4}	⋯	3.3×10^{-16}	
5	Kominis *et al.* (2003)	OPM	4.0×10^{-2}	4.0×10^{-3}	3.1×10^{-3}	3.0×10^{-7}	⋯	⋯	5.4×10^{-16}	
6	Sheng *et al.* (2013)	OPM	⋯	⋯	⋯	6.6×10^{-7}	⋯	⋯	5.4×10^{-16}	
7	Schmelz *et al.* (2011)	SQUID	7.0×10^{-3}	7.0×10^{-3}	⋯	⋯	4.9×10^{-5}	⋯	7.0×10^{-16}	
8	Drung, Knappe, and Koch (1995)	SQUID	7.3×10^{-3}	7.3×10^{-3}	⋯	⋯	4.4×10^{-5}	⋯	9.0×10^{-16}	
9	Faley *et al.* (2006, 2012, 2013)	SQUID	1.6×10^{-2}	1.6×10^{-2}	⋯	⋯	2.6×10^{-4}	⋯	3.5×10^{-15}	
10	Griffith, Knappe, and Kitching (2010)	OPM	1.0×10^{-3}	1.0×10^{-3}	1.0×10^{-3}	1.0×10^{-9}	⋯	⋯	5.0×10^{-15}	
11	Brandt and Mikitik (2000) and Pannetier *et al.* (2004)	GMR	4.4×10^{-4}	4.4×10^{-4}	⋯	⋯	1.9×10^{-7}	⋯	3.2×10^{-14}	
12	Luomahaara *et al.* (2014)	SKIM	2.0×10^{-2}	2.0×10^{-2}	⋯	⋯	4.0×10^{-4}	⋯	3.2×10^{-14}	
13	Krey, Barthelmess, and Schilling (1999)	SQUID	3.0×10^{-3}	3.0×10^{-3}	⋯	⋯	9.0×10^{-6}	⋯	8.5×10^{-14}	
14	Fong *et al.* (2005)	SQUID	1.0×10^{-3}	1.0×10^{-3}	⋯	⋯	7.9×10^{-7}	⋯	1.5×10^{-13}	
15	Fong *et al.* (2005)	SQUID	5.0×10^{-4}	5.0×10^{-4}	⋯	⋯	2.0×10^{-7}	⋯	2.4×10^{-13}	
16	Awschalom *et al.* (1988)	SQUID	2.5×10^{-5}	2.5×10^{-5}	⋯	⋯	6.3×10^{-10}	1.7×10^{-22}	2.8×10^{-13}	
17	Fong *et al.* (2005)	SQUID	5.0×10^{-4}	5.0×10^{-4}	⋯	⋯	2.0×10^{-7}	⋯	3.3×10^{-13}	
18	Vetoshko, Valeiko, and Nikitin (2003) and Robbes (2006)	YIG	1.0×10^{-2}	1.0×10^{-2}	⋯	⋯	1.0×10^{-4}	⋯	4.0×10^{-13}	
19	Fong *et al.* (2005)	SQUID	2.5×10^{-4}	2.5×10^{-4}	⋯	⋯	4.9×10^{-8}	⋯	4.5×10^{-13}	
20	Vengalattore *et al.* (2007)	BEC	1.1×10^{-5}	1.1×10^{-5}	⋯	⋯	1.2×10^{-10}	⋯	5.0×10^{-13}	
21	Crepaz, Ley, and Dumke (2015)	CEOPM	2.8×10^{-2}	2.8×10^{-2}	2.8×10^{-2}	1.1×10^{-5}	⋯	⋯	6.9×10^{-13}	
22	Fong *et al.* (2005)	SQUID	2.5×10^{-4}	2.5×10^{-4}	⋯	⋯	4.9×10^{-8}	⋯	8.5×10^{-13}	
23	Wolf *et al.* (2015)	RFNVD	9.5×10^{-5}	9.5×10^{-5}	9.5×10^{-5}	8.5×10^{-13}	⋯	⋯	9.0×10^{-13}	See also Zhou *et al.* (2019)
24	Fescenko *et al.* (2019)	FCNVD	1.0×10^{-2}	1.0×10^{-2}	2.0×10^{-2}	2.6×10^{-7}	⋯	⋯	9.0×10^{-13}	
25	Fong *et al.* (2005)	SQUID	4.0×10^{-5}	4.0×10^{-5}	⋯	⋯	1.6×10^{-9}	⋯	1.5×10^{-12}	
26	Kawai *et al.* (2016)	SQUID	2.0×10^{-4}	2.0×10^{-4}	⋯	⋯	4.0×10^{-8}	⋯	1.7×10^{-12}	
27	Cromar and Carelli (1981)	SQUID	4.0×10^{-5}	3.5×10^{-7}	⋯	⋯	1.4×10^{-11}	3.6×10^{-23}	2.6×10^{-12}	
28	Oda *et al.* (2016)	SQUID	2.0×10^{-4}	2.0×10^{-4}	⋯	⋯	4.0×10^{-8}	⋯	3.0×10^{-12}	
29	Cromar and Carelli (1981) and Van Harlingen, Koch, and Clarke (1982)	SQUID	3.0×10^{-5}	3.5×10^{-7}	⋯	⋯	1.1×10^{-11}	3.9×10^{-23}	3.8×10^{-12}	
30	Wood *et al.* (2015)	BEC	4.7×10^{-5}	2.1×10^{-5}	2.1×10^{-5}	2.0×10^{-14}	⋯	⋯	3.9×10^{-12}	
31	Schwindt *et al.* (2007)	OPM	1.0×10^{-3}	2.0×10^{-3}	1.0×10^{-3}	2.0×10^{-9}	⋯	⋯	5.0×10^{-12}	
32	Sewell *et al.* (2012)	COPM	2.0×10^{-5}	2.0×10^{-5}	3.0×10^{-3}	3.7×10^{-12}	⋯	⋯	5.4×10^{-12}	
33	Wang *et al.* (2012)	MFME	3.0×10^{-2}	2.0×10^{-3}	2.0×10^{-4}	1.2×10^{-8}	⋯	⋯	6.2×10^{-12}	
34	Schmelz *et al.* (2017)	SQUID	5.0×10^{-6}	5.0×10^{-6}	⋯	⋯	2.5×10^{-11}	3.1×10^{-22}	1.3×10^{-11}	
35	Schmelz *et al.* (2017)	SQUID	3.0×10^{-6}	3.0×10^{-6}	⋯	⋯	9.0×10^{-12}	1.4×10^{-22}	1.4×10^{-11}	
36	Jasperse *et al.* (2017)	BEC	⋯	⋯	⋯	2.9×10^{-14}	⋯	⋯	1.0×10^{-11}	
37	Eto *et al.* (2013)	BEC	1.0×10^{-5}	10.0×10^{-6}	⋯	⋯	1.0×10^{-10}	⋯	1.2×10^{-11}	
38	Barry *et al.* (2016)	NVD	1.3×10^{-5}	2.0×10^{-4}	2.0×10^{-3}	5.2×10^{-12}	⋯	⋯	1.5×10^{-11}	
39	Schmelz *et al.* (2017)	SQUID	1.0×10^{-6}	1.0×10^{-6}	⋯	⋯	1.0×10^{-12}	9.3×10^{-23}	3.6×10^{-11}	
40	Kim and Savukov (2016)	FCOPM	2.5×10^{-4}	5.0×10^{-4}	⋯	⋯	1.3×10^{-7}	⋯	2.3×10^{-11}	
41	Marauska *et al.* (2013)	MFME	2.0×10^{-4}	9.0×10^{-4}	⋯	⋯	1.8×10^{-7}	⋯	2.7×10^{-11}	

(Table continued)

TABLE I. *(Continued)*

Label	References	Type	l_1 (m)	l_2 (m)	l_3 (m)	V (m^3)	A (m^2)	$\delta\Phi\sqrt{T}$ ($T/\sqrt{Hz}$)	$\delta B\sqrt{T}$ ($Wb/\sqrt{Hz}$)	Notes
42	Schwindt *et al.* (2004)	OPM	1.0×10^{-3}	1.0×10^{-3}	1.0×10^{-3}	1.0×10^{-9}	⋯	⋯	5.0×10^{-11}	
43	Dietsche *et al.* (2019)	RSC	5.0×10^{-3}	2.8×10^{-7}	⋯	⋯	1.4×10^{-9}	⋯	5.8×10^{-11}	
44	Ockeloen *et al.* (2013)	BEC	1.1×10^{-6}	1.1×10^{-6}	4.0×10^{-6}	2.0×10^{-17}	⋯	⋯	7.7×10^{-11}	
45	Robbes (2006)	EMR	5.0×10^{-5}	5.0×10^{-5}	⋯	⋯	2.5×10^{-9}	⋯	1.0×10^{-10}	
46	Gallop *et al.* (2002)	SQUID	3.0×10^{-6}	3.0×10^{-6}	⋯	⋯	9.0×10^{-12}	1.0×10^{-21}	1.1×10^{-10}	
47	Jeng, Chen, and Lu (2012)	PAFG	8.0×10^{-3}	1.0×10^{-3}	1.5×10^{-5}	1.2×10^{-10}	⋯	⋯	1.8×10^{-10}	
48	Wildermuth *et al.* (2004, 2005, 2006)	BEC	3.0×10^{-6}	3.0×10^{-6}	3.0×10^{-6}	2.7×10^{-17}	⋯	⋯	2.3×10^{-10}	
49	Clevenson *et al.* (2015)	NVD	3.0×10^{-3}	3.0×10^{-3}	3.0×10^{-4}	2.7×10^{-9}	⋯	⋯	2.9×10^{-10}	
50	Hankard *et al.* (2009)	GMR	9.0×10^{-6}	3.6×10^{-5}	⋯	⋯	3.2×10^{-10}	⋯	3.0×10^{-10}	
51	Behbood *et al.* (2013)	COPM	5.0×10^{-3}	2.0×10^{-5}	2.0×10^{-5}	2.0×10^{-12}	⋯	⋯	3.2×10^{-10}	
52	Giazotto *et al.* (2010)	SQUIPT	1.1×10^{-5}	1.1×10^{-5}	⋯	⋯	1.2×10^{-10}	4.1×10^{-20}	3.4×10^{-10}	
53	Wakai and Van Harlingen (1988)	SQUID	3.3×10^{-6}	6.7×10^{-6}	⋯	⋯	2.2×10^{-11}	1.1×10^{-20}	5.1×10^{-10}	
54	Kirtley *et al.* (2016)	SQUID	2.0×10^{-6}	2.0×10^{-6}	⋯	⋯	3.1×10^{-12}	4.1×10^{-21}	1.3×10^{-9}	
55	Muessel *et al.* (2014)	BEC	2.5×10^{-4}	1.5×10^{-6}	1.5×10^{-6}	9.0×10^{-17}	⋯	⋯	1.9×10^{-9}	
56	Ahmadi *et al.* (2017)	NVD	1.8×10^{-5}	1.8×10^{-5}	3.1×10^{-3}	3.5×10^{-11}	⋯	⋯	3.0×10^{-9}	
57	Kirtley (2010)	SQUID	6.5×10^{-7}	6.5×10^{-7}	⋯	⋯	4.2×10^{-13}	1.8×10^{-21}	4.3×10^{-9}	
58	Vasyukov *et al.* (2013)	SQUID	1.6×10^{-7}	1.6×10^{-7}	⋯	⋯	2.0×10^{-14}	1.0×10^{-22}	5.1×10^{-9}	
59	Yang *et al.* (2017)	BEC	2.0×10^{-6}	2.0×10^{-6}	⋯	⋯	4.0×10^{-12}	⋯	6.0×10^{-9}	
60	Fang *et al.* (2013)	RFNVD	5.0×10^{-7}	⋯	⋯	⋯	⋯	⋯	3.8×10^{-8}	
61	Vasyukov *et al.* (2013)	SQUID	5.6×10^{-8}	5.6×10^{-8}	⋯	⋯	2.5×10^{-15}	1.0×10^{-22}	4.2×10^{-8}	
62	Lovchinsky *et al.* (2016)	RFNVD	4.0×10^{-9}	⋯	⋯	⋯	⋯	⋯	5.3×10^{-8}	
63	Maletinsky *et al.* (2012)	RFNVD	2.5×10^{-8}	⋯	⋯	⋯	⋯	⋯	5.6×10^{-8}	
64	Vasyukov *et al.* (2013)	SQUID	4.6×10^{-8}	4.6×10^{-8}	⋯	⋯	1.7×10^{-15}	1.0×10^{-22}	6.2×10^{-8}	
65	Huang *et al.* (2014)	GRA	1.6×10^{-4}	1.6×10^{-4}	⋯	⋯	2.6×10^{-8}	⋯	1.0×10^{-7}	
66	Bending (1999)	HALL	2.0×10^{-7}	2.0×10^{-7}	⋯	⋯	4.0×10^{-14}	⋯	1.0×10^{-7}	
67	Lovchinsky *et al.* (2016)	RFNVD	3.0×10^{-9}	⋯	⋯	⋯	⋯	⋯	1.0×10^{-7}	
68	Lovchinsky *et al.* (2016)	RFNVD	5.0×10^{-9}	⋯	⋯	⋯	⋯	⋯	1.1×10^{-7}	
69	Forstner *et al.* (2014)	WGM	4.0×10^{-5}	4.0×10^{-5}	4.0×10^{-5}	6.5×10^{-14}	⋯	⋯	1.4×10^{-7}	
70	Lima *et al.* (2014)	MTJ	7.0×10^{-6}	7.0×10^{-6}	⋯	⋯	4.9×10^{-11}	⋯	1.5×10^{-7}	
71	Zhou *et al.* (2019)	RFNVD	1.3×10^{-7}	1.5×10^{-7}	1.3×10^{-7}	8.1×10^{-21}	⋯	⋯	2.2×10^{-7}	
72	Trusheim *et al.* (2014)	RFNVD	5.0×10^{-8}	5.0×10^{-8}	5.0×10^{-8}	1.3×10^{-22}	⋯	⋯	2.9×10^{-7}	
73	Chenaud *et al.* (2016)	HALL	1.0×10^{-6}	1.0×10^{-6}	⋯	⋯	1.0×10^{-12}	⋯	3.0×10^{-7}	
74	Oral *et al.* (2002)	HALL	1.5×10^{-6}	1.5×10^{-6}	⋯	⋯	2.3×10^{-12}	⋯	6.0×10^{-7}	
75	Maletinsky *et al.* (2012)	NVD	2.5×10^{-8}	⋯	⋯	⋯	⋯	⋯	6.0×10^{-6}	
76	Kirtley (2010)	MFM	1.0×10^{-8}	1.0×10^{-8}	⋯	⋯	1.0×10^{-16}	7.0×10^{-20}	7.0×10^{-4}	

B. Alkali-vapor optically pumped magnetometers

Hot-vapor OPMs (Budker and Romalis, 2007; Jensen, Kehayias, and Budker, 2017; Jiménez-Martínez and Knappe, 2017; Savukov, 2017; Weis, Bison, and Grujić, 2017) have also been shown to obey a volumetric energy resolution limit. In these devices, quantum noise in the form of optical shot noise, optical spin-rotation noise, and spin projection noise all contribute to the effective magnetic noise (Smullin *et al.*, 2009) and scale differently with atomic number density, volume, and optical probe power. When optimized for sensitivity, and in the most sensitive, spin-exchange-relaxation-free regime, the equivalent magnetic noise is limited by

$$S_B(0) \geq \frac{1}{\gamma^2}\frac{\bar{v}\sigma_{\mathrm{SD}}}{V}, \tag{7}$$

where γ is the gyromagnetic ratio, $\bar{v}$ is the thermal velocity, σ_{SD} is the cross section for spin-destruction collisions, and V is the volume of the sensor (Jiménez-Martínez and Knappe, 2017). When expressed in terms of the field energy, this quantum limit is

$$\frac{S_B(0)V}{2\mu_0} \geq \frac{\bar{v}\sigma_{\mathrm{SD}}}{2\mu_0\gamma^2}. \tag{8}$$

Spin-destruction collisions result when spin angular momentum is transferred to the center-of-mass degree of freedom. In ^{87}Rb, the limiting energy resolution is nearly $\hbar$ when calculated using measured spin-destruction rates (Jiménez-Martínez and Knappe, 2017). This agreement with the E_R of dc SQUIDs appears to be a coincidence, as other alkali species and noble gases have significantly lower values for $\bar{v}\sigma_{\mathrm{SD}}\gamma^{-2}$; see Sec. VII.E. Realized OPMs using ^{87}Rb and K have demonstrated E_R as low as $44\hbar$ (Allred *et al.*, 2002; Savukov *et al.*, 2005; Shah *et al.*, 2007; Ledbetter *et al.*, 2008; Smullin *et al.*, 2009; Dang, Maloof, and Romalis, 2010), limited by environmental noise.

C. Immobilized spin ensembles: Nitrogen-vacancy centers in diamond

In contrast to OPMs, which employ mobile spins in the vapor phase, sensors employing NV centers in diamond use immobile spins fixed in a solid matrix (Acosta *et al.*, 2013; Doherty *et al.*, 2013; Rondin *et al.*, 2014). In this scenario, no entropy is input into the spin system by collisions, and decoherence due to nuclear spins (Taylor *et al.*, 2008) can, in principle, be fully eliminated by use of isotopically pure ^{12}C diamond (Balasubramanian *et al.*, 2009). Nonetheless, the spins necessarily interact with each other by dipole-dipole coupling, and this interaction allows angular momentum loss to the crystal lattice. A recent analysis of the limiting sensitivity imposed by this effect (Mitchell, 2020) finds that for spatially disordered spins dipolar coupling of the sensor spins themselves is sufficient to cause depolarization and enforce Eq. (6) with $\alpha \approx 1/2$.

VI. POSSIBLE SOURCES OF TECHNOLOGY-INDEPENDENT LIMITS

The fact that three different sensor technologies all arrive at the same limit again suggests that there could be a more general reason for energy resolution to be limited to $\hbar$. As examples, the magnetic field itself is subject to quantum fluctuations, and any system measuring the field must obey quantum speed limits. In this section, we evaluate several general considerations that could give rise to a technology-spanning ERL.

A. Standard quantum limit, Heisenberg limit, and amplification quantum noise

A considerable literature has developed around the topic of "quantum-enhanced sensing" (Giovannetti, Lloyd, and Maccone, 2004; Braun *et al.*, 2018; Pezzè *et al.*, 2018), which explores the use of nonclassical states to achieve sensitivity between the standard quantum limit (SQL) and the so-called Heisenberg limit (HL). These limits are defined in terms of the number of particles employed in the sensing procedure. For example, the SQL for measurement of a phase angle ϕ with N noninteracting two-level systems is $\langle \delta\phi^2 \rangle = N^{-1}$. It is notable that the ERL makes no reference to particle number, whereas the SQL and HL make no reference to spatial extent or time. Any derivation of the ERL from the SQL or HL would thus require important input from other physical principles.

Similarly, linear, phase-insensitive amplification is known to introduce quantum noise intrinsic to the amplification process (Caves, 1982). This noise, when present, has a magnitude similar to the intrinsic quantum noise of the system to be measured, resulting in an equivalent noise comparable in magnitude to the SQL. As such, amplification quantum noise is not, *per se*, an explanation of the ERL.

B. Energy-time uncertainty relation

The energy-time uncertainty relation $\delta E \delta t \geq \hbar/2$ is the paradigmatic example of an uncertainty relation not derived using the commutation relation of the involved quantities. The same form of the energy-time uncertainty relation is found in a variety of scenarios with different meanings for t, for example, in the question of arrival-time distributions (Aharonov and Bohm, 1961) or in the estimation of a Hamiltonian in limited time (Aharonov, Massar, and Popescu, 2002). The latter problem is closely related to quantum estimation methods (Helstrom, 1969; Giovannetti, Lloyd, and Maccone, 2004), in which δt is the measurement duration, i.e., T. Using this definition and taking E to be the magnetostatic energy $VB^2/(2\mu_0)$, we find

$$\frac{\delta(B^2)VT}{2\mu_0} \geq \frac{1}{2}\hbar, \tag{9}$$

which differs from Eq. (5) in that it contains the rms deviation of B^2 rather than the variance of B. This is an important difference: considering a small uncertainty δB on a large field $B \gg \delta B$, $\delta(B^2) \approx 2B\delta B$ so that Eq. (9) allows for arbitrarily small δB as $B \to \infty$. It would appear that the energy-time uncertainty relation places no limit on magnetic sensitivity.

C. Zero-point and thermal field fluctuations

To our knowledge, not much attention has been paid to the possibility that the quantum fluctuations of the magnetic field might be detectable and thus a source of noise for sensitive magnetometry. One can imagine a scenario in which the goal is precisely to observe the zero-point fluctuations, in which case these fluctuations are not noise, but rather signal. Such a measurement has indeed been reported with terahertz electric fields (Tighineanu *et al.*, 2014; Riek *et al.*, 2015). For our purposes, however, we are more interested in the effect of zero-point fluctuations when measuring fields of material origin, e.g., from a current. In such a measurement, the zero-point fluctuations would be considered noise if indeed they contribute to the recorded signal.

In Appendix A, we analyze the following model for the effect of zero-point fluctuations. First, we define a spherical region $\mathcal{R}$ of radius r_S and volume V, and the $\mathcal{R}$-averaged field component $\bar{B}_z(t) \equiv V^{-1} \int d^3 r \rho(\mathbf{r}) B_z(\mathbf{r}, t)$, where $\rho(\mathbf{r})$ is a weighting function. At any value of the time t, $\bar{B}_z(t)$ is an Hermitian operator and thus a valid quantum mechanical observable. An ideal measurement of this observable will have a mean that is the true spatially averaged value of any externally applied field in that region, and finite contribution to the variance from zero-point fluctuations. Measurement of this observable will also produce a random and, in principle, unbounded measurement backaction in the conjugate electric field $\mathbf{E}$, which through the Maxwell equations will propagate into $\mathbf{B}$. Nonetheless, due to the space-bounded nature of the measurement, and the fact that EM fields propagate at speed c, all effects of this disturbance will propagate out of the volume of interest after a time $T_{\text{eff}} = 2r_S/c$, at which point a measurement of $\bar{B}(t + T_{\text{eff}})$ with independent noise can be made. Considering a sequence of such measurements separated by T_{eff}, we find a zero-point-limited energy resolution

$$E_R \geq \alpha\hbar, \tag{10}$$

where $\alpha \approx 1.3$ for the specific weighting considered; see Eq. (A2). This is not far from other derived energy resolution limits. In the same analysis, we consider thermal fields and find a contribution to E_R of $\approx r_s k_B T_B / c$, where T_B is the field temperature.

However elegant such a solution to the energy resolution question might appear, we believe that it hides a subtle and incorrect assumption and does not represent a fundamental limit. If we replace the "ideal measurement" of $\bar{B}$ with a more detailed model of the measurement, the problem becomes apparent. Imagine that we fill the region $\mathcal{R}$ with a rigid sphere of zero temperature, uniformly magnetized material (e.g., a single ferromagnetic domain). We assume that the energy of the ferromagnet is independent of its spin direction, and that it is "stiff" in the sense that all regions must share a single spin orientation. The measurement consists of allowing this object to freely rotate in response to the field it experiences, then observing its new orientation. If the initial state of this evolution is a product of the ground state of the magnet and the ground state of the field (vacuum), we would indeed observe a random rotation, a noise signal due to the zero-point magnetic field. If, on the other hand, we take as our initial condition the minimum-energy state of the coupled field-ferromagnet system, we would, simply because we are considering an energy eigenstate, observe no rotation, or indeed change of any kind. From such an initial condition, any rotation of the system, even if stochastic, would at least temporarily violate angular momentum conservation. See Appendix B for a more detailed discussion of this point. We conclude that this in-principle-possible magnetic sensor, embedded in vacuum and allowed to find equilibrium with it, would not experience a noise from vacuum fluctuations.

D. Spin intrinsic-noise self-interaction

Any spin ensemble will have intrinsic uncertainty in its net spin $\mathbf{J}$ as a consequence of spin uncertainty relations. If the ensemble spins are associated with a magnetic moment, the magnetic field produced by the ensemble will similarly have an intrinsic uncertainty. The possibility that this uncertain field acts back on the ensemble and introduces a self-interaction noise has been discussed in the OPM community (Lee and Romalis, 2008; Kitching, 2012; Lee, 2019). Here we consider a simple model of this hypothetical noise source.

We consider a spherical region occupied by $N \gg 1$ spin-1/2 atoms with a total spin $J = N/2$, initially polarized along the z axis, so that $\langle J_z \rangle \approx N/2$. We note that the J_x and J_y components of the total spin vector obey the uncertainty relation $\delta J_x \delta J_y \geq |\langle J_z \rangle|/2 \approx N/4$. Considering precession about the y axis for a time T as a measure of the field component B_y, we can associate the uncertainty δJ_x with an angular uncertainty $\delta\theta = \delta J_y / \langle J_z \rangle$, and thus a magnetic field uncertainty

$$\delta B_{\mathrm{SPN}} = \frac{\delta J_x}{\langle J_z \rangle \gamma T} \geq \frac{2}{\gamma T \delta J_y}, \tag{11}$$

where $\gamma = g_J \mu_B$ is the gyromagnetic ratio and SPN indicates spin projection noise.

δJ_y can also be associated with a field uncertainty through the magnetic field generated by the ensemble of spins. Modeling the ensemble as a uniformly magnetized sphere, we find that the self-generated field inside the sphere is $\mathbf{B} = 2\mu_0 \mathbf{M}/3$, where $\mathbf{M} = \hbar\gamma \mathbf{J}/V$ is the magnetization density of the material (Griffiths, 1999). As we are interested in just the B_y component, we have

$$\delta B_{\mathrm{MSI}} = \frac{2\hbar\gamma\mu_0 \delta J_y}{3V}, \tag{12}$$

where MSI indicates magnetic self-interaction.

If we suppose that these two noise sources are independent, the energy resolution per bandwidth is

$$\begin{aligned} E_R &= \frac{\langle \delta B^2 \rangle VT}{2\mu_0} = \frac{\langle \delta B^2_{\mathrm{SPN}} \rangle + \langle \delta B^2_{\mathrm{MSI}} \rangle}{2\mu_0} VT \\ &\geq \frac{C^2 x^{-1} + D^2 x}{2\mu_0} \geq \frac{CD}{\mu_0} = \frac{4}{3}\hbar, \end{aligned} \tag{13}$$

where $C \equiv 2/\gamma$, $D \equiv 2\hbar\gamma\mu_0/3$, and $x \equiv T\langle \delta J_y^2 \rangle / V$. The first inequality is saturated for minimum uncertainty states, i.e., those with $\delta J_x \delta J_y = |\langle J_z \rangle|/2$, and the second can be saturated by choosing T such that $C^2 x^{-1} = D^2 x$.

As was the case with zero-point fluctuations, the result is consistent with observed values of E_R. As in that case, here also we find that the calculation is subtly misleading and does not in fact represent a limit. For one thing, the precession angle, and thus B_y, can be inferred from a measurement of a single spin component, e.g., J_x if the precession angle is small. The noise in J_x and the noise in J_y, if it contributes to the rotation speed, will contribute in linear combination to the field estimate. There will be spin-squeezed states that have small uncertainty of this linear combination, producing a total noise $\langle \delta B^2 \rangle$ much smaller than the $\langle \delta B^2_{\mathrm{SPN}} \rangle + \langle \delta B^2_{\mathrm{MSI}} \rangle$ that appears in Eq. (13). In a few words, the sum in quadrature is not appropriate if J_x and J_y are correlated.

A still more serious objection is that magnetic self-action of the kind assumed here, like the vacuum field effects described in Sec. VI.C, appears unphysical. The previous model suggests that, in the absence of any external field, a spin system could reorient itself to have a net angular momentum different from its initial angular momentum. Indeed, given enough time, it would sample all possible orientations. This kind of "bootstrapping," in which the spin system rotates itself does not conserve angular momentum (we note that the spin system has no neighbors with which to exchange angular momentum). The possibility that the angular momentum is taken up by the electromagnetic field suggests itself, but this would seem to violate energy conservation, as the spin system would forever radiate a fluctuating field.

E. Margolus-Levitin bound

If we consider the magnetometer and field together as a single quantum system, the Margolus-Levitin (ML) theorem (Margolus and Levitin, 1998) shows that this system cannot change from an initial state $|\psi_i\rangle$ to an orthogonal final state $|\psi_f\rangle$ in a time shorter than

$$T_{\min} = \frac{\pi\hbar}{2E}, \tag{14}$$

where $E \equiv \langle H\rangle - E_0$ is the mean available energy, H is the Hamiltonian, and E_0 is its lowest eigenvalue. If we identify E with $B^2V/(2\mu_0)$, i.e., the magnetic field energy within the sensor volume V, we can identify a minimum field strength $B_{\min}$ that produces orthogonality in time $T_{\min}$ and thus can reliably be distinguished from zero field. This gives

$$\frac{B_{\min}^2 V T_{\min}}{2\mu_0} \geq \frac{\pi\hbar}{2}, \tag{15}$$

which resembles an ERL, with the difference that the squared field appears rather than the mean squared error of the field estimate.

As with the energy-time uncertainty relation discussed previously, this difference is important: If we consider a small perturbation δB to a large field B_0, it would be natural to divide the total energy into a fixed contribution $E_0 = B_0^2V/(2\mu_0)$ and the perturbation to the energy $\langle H\rangle \approx 2\delta B B_0 V/(2\mu_0)$, leading to

$$\frac{\delta B B_0 V T_{\min}}{\mu_0} \geq \frac{\pi\hbar}{2}, \tag{16}$$

which for large B_0 allows detection of $\delta B \ll B_{\min}$. Another serious concern for use of the ML bound to derive an ERL is the role of field-matter coupling. For example, a sensor with magnetic moment μ would contribute $-\mu\cdot\mathbf{B}$ to the total energy. If this is included in E and μ is allowed to become large, the minimum detectable field can vanish.

F. Bremermann-Bekenstein bound

In the context of black hole thermodynamics (Wald, 1979), it was shown by Bremermann and Bekenstein (BB) (Bekenstein, 1981b; Bremermann, 1982) that a spherical region $\mathcal{R}$ with radius R contains a bounded information entropy

$$H_{\mathrm{BB}} \leq \frac{2\pi E R}{\hbar c}, \tag{17}$$

where E is the mean energy contained in the sphere. The result applies also to nonrelativistic scenarios (Schiffer, 1991) and has been applied to the question of the energy cost of communication (Bekenstein, 1981a, 1984) by considering moving packets of material and/or radiation, echoing earlier bounds based on Shannon information capacity and energy-time uncertainty (Bremermann, 1982).

We may consider the readout of the sensor as communication from the sensor to some other system, which might be a display, a recording device, or an interested scientist. As for the ML bound, it is natural to consider the magnetostatic field energy $E = \langle B^2\rangle V/(2\mu_0)$. The entropy we interpret as an upper bound on the number of resolvable field states. One bit of message, corresponding to the minimum detectable field $B_{\min}$, is then achieved for a field energy

$$\frac{2\pi\langle B_{\min}^2\rangle V R}{2\mu_0 c} \geq \hbar. \tag{18}$$

We note that at the maximum speed of communication c information requires at least $T_{\mathrm{eff}} = R/c$ to reach a single point from the entirety of $\mathcal{R}$. Inserting this into Eq. (18) we find

$$\frac{\langle B_{\min}^2\rangle V T_{\mathrm{eff}}}{2\mu_0} \geq \frac{1}{2\pi}\hbar, \tag{19}$$

which resembles an ERL, with the difference being that the mean squared field appears rather than the mean squared error of the field estimate. As with the ML bound, this appears to allow resolution of small increments on large fields.

The nonlinearity implicit in Eq. (17), in which H_{BB} is both the logarithm of the number of possible states and proportional to the mean squared field, amplifies this concern. We take as a reference a spherical region $\mathcal{R}$ containing a field B with $\langle B^2\rangle = B_{\min}^2$, sufficient to encode 1 bit of information or, equivalently, to distinguish between two possible field states. If we now imagine the same region containing a stronger field, with $\langle B^2\rangle = \beta^2 B_{\min}^2$ for some $\beta > 1$, Eq. (17) limits the entropy to $H_{\mathrm{BB}} = \beta^2$ bits, which can encode up to 2^{β^2} distinct states distributed over the $\sim\beta B_{\min}$ range of the field distribution. The minimum resolvable field increment δB is then

$$\frac{\delta B}{B_{\min}} \sim \sqrt{\frac{\langle B^2\rangle}{B_{\min}^2}}\exp\left[-\frac{\langle B^2\rangle}{B_{\min}^2}\right]. \tag{20}$$

This describes an exponentially small minimum field increment, achieved when measuring large (or potentially large) fields.

VII. SYSTEMS PROPOSED TO SURPASS $E_R = \hbar$

We have described both established technology-specific and potential technology-spanning quantum limits on the energy resolution. No convincing technology-spanning limit was found, however, leaving open the possibility of sensing with unconstrained energy resolution. In this section, we describe sensing methods, both proposed and implemented, that appear to evade the technology-specific quantum limits presented previously.

A. Nondissipative superconducting sensors

The TC limit arises due to the zero-point current fluctuations in the shunt resistances, the only dissipative components of the dc SQUID model analyzed by Tesche and Clarke. A sufficiently small shunt resistance prevents hysteresis, making the SQUID current a single-valued function of the flux to be detected. The intrinsic noise of the dc SQUID could, within this model, vanish if the resistance were made infinite. The interpretation of the current signal would, however, be more complex. Superconducting field sensors that do not include a dissipative element include superconducting quantum interference proximity transistors (SQUIPTs) (Giazotto *et al.*, 2010) and superconducting kinetic inductance magnetometers

(Kher *et al.*, 2013, 2016; Luomahaara *et al.*, 2014; Kher, 2017). Superconducting persistent current qubits (Bal *et al.*, 2012) and transmon qubits (Danilin *et al.*, 2018) have also been studied as nondissipative superconducting sensors.

B. Localized single quantum systems

Single quantum systems (SQSs) such as NV centers (Taylor *et al.*, 2008) and single trapped ions (Baumgart *et al.*, 2016) have been proposed as extremely-high-spatial-resolution field sensors. Single Rydberg atoms have also been studied as magnetic sensors (Dietsche *et al.*, 2019). Because they are elementary systems, internal decoherence mechanisms such as those described in Secs. V.B and V.C can be fully evaded. These sensors are also potentially small, with the effective linear dimension limited by the precision with which they can be localized and the minimum distance from possible sources. It thus seems possible that SQSs would have no energy resolution limit. It is, nonetheless, worth noting that SQSs in solids experience significant noise from surface effects (Myers, Ariyaratne, and Jayich, 2017), an effect that becomes more important as effective linear dimension decreases. Similarly, efforts to produce small ion traps have uncovered important noise sources associated with closely placed electrodes (Hite *et al.*, 2013).

C. Dynamical decoupling and low-entropy reservoirs

As described in Sec. V.C, fixed, spatially disordered spin ensembles (e.g., NVD ensembles as currently implemented) experience a self-depolarization caused by the magnetic dipole-dipole coupling among elements of the ensemble. This depolarization can be understood as a transfer entropy from the center-of-mass (c.m.) degrees of freedom into the spin degrees of freedom by a coherent evolution that is not a source of entropy *per se*.

Two classes of methods present themselves to prevent such dipole-induced depolarization. The first, more established method is dynamical decoupling (Viola and Lloyd, 1998), in which strong, impulsive spin operations are applied to prevent or reverse the buildup of coherent rotations due to the naturally present dipolar coupling. Such decoupling of sensing electrons from a surrounding bath of nuclear spins is an established method, e.g., with NVD (Pham *et al.*, 2012). The application to an ensemble of sensor spins has the potential to dynamically decouple the spins from their neighbors while leaving them coupled to the external field to be measured (Choi, Yao, and Lukin, 2017). The theory and design of suitable pulse sequences is an active topic (Ben 'Attar, Farfurnik, and Bar-Gill, 2019; Choi *et al.*, 2019; Haas *et al.*, 2019), and experimental results have been reported (Zhou *et al.*, 2019).

The second approach is simply to remove the entropy from the reservoir, which could, in principle, be done by ordered positioning of the spins. Similarly, phononic disorder can be reduced through cooling, although even at zero temperature the phononic vacuum presents a decoherence channel (Astner *et al.*, 2018).

Another possible route to entropy removal in spin-precession sensors is the use of quantum degenerate gases. In such a system (a spinor BEC), two-body interactions, including both short-range ferromagnetic or antiferromagnetic contact interactions and long-range dipole-dipole coupling, induce coherent spin evolutions rather than introducing entropy to the spins. A jump in coherence lifetime at Bose-Einstein condensation has been observed in planar geometries (Higbie *et al.*, 2005) and exploited for high-sensitivity BEC magnetic imagers (Vengalattore *et al.*, 2007) and gradiometers (Vengalattore *et al.*, 2007; Wood *et al.*, 2015; Jasperse *et al.*, 2017). A full "freezing-out" of the c.m. degrees of freedom has been observed in a quasi-zero-dimensional single-domain spinor BEC (Palacios *et al.*, 2018). These results were all obtained with the ferromagnetic ground state of ^{87}Rb.

D. Precessing ferromagnetic needle

A similar freezing-out of nonspin degrees of freedom is predicted for solid-state ferromagnets in the single-domain size regime (Jackson Kimball, Sushkov, and Budker, 2016). As with the BEC case described previously, the ferromagnetic interactions impose full polarization, and at low temperatures no intrinsic fluctuations cause diffusion of the polarization angle. Assuming that background gas pressure, which imparts random angular momentum input, can be arbitrarily reduced, the sensitivity limited by readout noise is predicted to scale as $\langle \delta B^2 \rangle T \propto T^{-2}$. Thus, for long measurements, E_R is predicted to have no lower limit in this system. Variants based on free rotation (Jackson Kimball, Sushkov, and Budker, 2016) and on normal mode oscillations (Vinante *et al.*, 2019) have been proposed.

E. OPMs with low spin-destruction rates

As described in Sec. V.B, the ERL arises in gas- and vapor-phase spin-precession magnetometers due to two-body relaxation processes, e.g., spin-destruction collisions, with a limit $E_R \geq \bar{v}\sigma/(2\mu_0\gamma^2)$, where σ is the relevant spin-relaxation cross section. The figure of merit $\bar{v}\sigma\gamma^{-2}$ varies considerably among alkali and noble gas species, with lower values for noble gases and lighter atoms (Newbury *et al.*, 1993; Kadlecek *et al.*, 2001; Chann *et al.*, 2002; Berry-Pusey *et al.*, 2006). σ_{SD} is about an order of magnitude lower for K than for ^{87}Rb (Allred *et al.*, 2002), such that the predicted ERL for a SERF-regime K vapor magnetometer is below $\hbar$. Generalization about two-body relaxation is difficult due to the coexistence of several mechanisms including transient dimer formation, spin-orbit coupling in second order, and magnetic dipole-dipole coupling (Kadlecek *et al.*, 2001). It is nonetheless instructive to consider the case of pure magnetic dipole-dipole relaxation, which appears to describe at least the case of gaseous ^{3}He at large pressures (Gentile *et al.*, 2017). For this mechanism, the spin-destruction cross section scales as $\sigma_{\mathrm{dd}} \propto \mu^4 \propto \gamma^4$, where μ is the atomic magnetic moment (Newbury *et al.*, 1993). As a result, the ERL figure of merit favors atomic species with small magnetic moments such as ^{3}He.

VIII. SUMMARY AND OBSERVATIONS

In this Colloquium, we have reviewed the history and status of energy resolution limits in precise sensing of low-frequency

magnetic fields. We now recapitulate our findings and comment on their significance to ongoing efforts to improve sensor performance. First, we have reviewed reported sensor performance, finding that the best reported sensors obey a limit $E_R \geq \hbar$, even as they span many orders of magnitude in size and field resolution. We conclude that E_R is, at a minimum, an interesting metric for comparing different technologies; it must in some meaningful way capture the challenges of achieving high sensitivity, speed, and spatial resolution. The fact that the best achieved values for E_R approach $\hbar$ is suggestive of a fundamental quantum limit.

This suggestion is backed up by technology-specific ERLs, which are known for dc SQUIDs, rubidium-vapor OPMs, and fixed-position spin-precession sensors, e.g., NVD sensors. These ERLs coincide in predicting a limit near $E_R = \hbar$. The origins of these ERLs are quite technology specific, involving shunt resistances, spin-destruction collisions, and random dipole-dipole couplings, respectively, and they have not yet been brought together under any unifying principle. We have reviewed several general quantum limits and their potential to supply a unifying, technology-spanning ERL. We have in fact found several arguments that could be made to predict a technology-spanning ERL near $\hbar$. In our analysis, however, each of these arguments has some important weakness, and none of them convincingly implies an ERL. Finally, we have reviewed proposed new sensor types and modifications to existing sensor methodologies, which appear to escape all of the known ERLs and thus may provide E_R values far below $\hbar$. Such sensors, if their current analyses are correct, have the potential to surpass today's leading magnetometer technologies.

The technology-specific ERLs each in some way concern dissipation mechanisms that are closely linked to the sensor's response to the applied field. In the case of dc SQUIDs, dissipation in the form of finite shunt resistance is introduced to achieve a single-valued steady-state response, i.e., to remove hysteresis. In alkali-vapor OPMs, the rate of alkali-induced spin-destruction collisions is proportional to the alkali number density, which directly impacts the projection-noise-limited signal-to-noise ratio. In color-center sensors, the dissipation is similarly linked to magnetic dipole-dipole coupling, and it has a similar dependence on number density. Viewed as a group, they can be summarized by the proposition: A useful coupling of the sensor to the field of interest necessarily also creates a dissipation strong enough to impose an ERL. In light of this, one can imagine a limit covering diverse technologies emerging from the theory of many-body open quantum systems (Davies, 1976; Ingarden, Kossakowski, and Ohya, 1997; Lindblad, 2001; Breuer and Petruccione, 2007; Rotter and Bird, 2015). To our knowledge, the question of ERLs has not been studied in that context.

The proposals for new, ERL-surpassing sensors aim for the most part to alter an existing sensor methodology in such a way that it evades the previously mentioned mechanisms that link field response to dissipation. For example, single quantum systems are predicted to retain sensitivity to external fields while evading completely dipole-dipole coupling of sensor components, simply because there is only one component. More generally, the specificity of the known ERLs makes it plausible that a sensing system could be designed to evade them. We thus find ourselves, at the end of this Colloquium, of two minds. On the one hand, the coincidence of multiple technology-specific quantum limits with each other, and with the empirical results of the most advanced sensor systems, makes it difficult to believe that there is not some as-yet-undiscovered general principle imposing ERLs on field sensors. At the same time, we do not see any fundamental impediment to sensors with arbitrarily small E_R if they are constructed to evade the existing limits. Perhaps the resolution to this dilemma is equally bifurcated: It may be that a broad class of sensors is subject to a yet-to-be-discovered ERL, while a second class, operating by other principles, escapes it. We hope that our observations in this Colloquium will help to resolve this and other open questions on the topic of sensor energy resolution limits, and that they will ultimately help to advance sensor technology.

ACKNOWLEDGMENTS

We thank J. Kitching for suggesting this problem, and for sharing his insights on several aspects of it, including unpublished work. M. Romalis and S.-K. Lee shared unpublished work on limits set by spin-destruction collisions and spin-noise self-interaction. We are grateful to the following people for their helpful comments: I. Chuang, M. Lukin, J. Wrachtrup, and H. Zhou (NVD sensors), M. Schmelz and R. Stolz (dc SQUIDs), J. Hassel and A. Lupascu (nondissipative superconducting sensors), D. Griffiths (classical magnetostatics), D. F. Jackson Kimball and H. Ulbricht (levitated magnetic sensors), and D. Budker (multiple topics). We thank R. J. Sewell for the feedback on the manuscript. This project was supported by H2020 Future and Emerging Technologies Quantum Technologies Flagship projects MACQSIMAL (Grant Agreement No. 820393) and QRANGE (Grant Agreement No. 820405); H2020 Marie Skłodowska-Curie Actions project ITN ZULF-NMR (Grant Agreement No. 766402); Spanish MINECO projects OCARINA (Grant No. PGC2018-097056-B-I00), Q-CLOCKS (Grant No. PCI2018-092973), and the Severo Ochoa program (Grant No. SEV-2015-0522); Generalitat de Catalunya through the CERCA program and RIS3CAT project QuantumCAT; Agència de Gestió d'Ajuts Universitaris i de Recerca Grant No. 2017-SGR-1354; Fundació Privada Cellex; 17FUN03-USOQS, which has received funding from the European Metrology Programme for Innovation and Research (EMPIR) program cofinanced by the Participating States and from the European Union's Horizon 2020 research and innovation program.

APPENDIX A: THERMAL AND ZERO-POINT MAGNETIC NOISE

We imagine a device that instantaneously makes an ideal measurement of the z component of the magnetic field, within a spherical region $\mathcal{R}$ of volume $V_s = 4\pi r_S^3/3$, where r_s is the radius of the region, which for convenience we take to be centered on the origin.

We describe this via the scalar observable

$$\bar{B}_z(t) \equiv \int d^3 r \rho(\mathbf{r}) \hat{z} \cdot \mathbf{B}(\mathbf{r}, t), \tag{A1}$$

where $\mathbf{B}(\mathbf{r},t)$ is the quantized magnetic field. The weighting function $\rho(\mathbf{r}) \geq 0$ should be normalized, $\int d^3r\rho(\mathbf{r}) = 1$, and should vanish for $r > r_S$, but it is otherwise arbitrary. In what follows, we use

$$\rho(\mathbf{r}) = \frac{5}{2V_S}\begin{cases} 1 - r^2/r_S^2, & r \leq r_S, \\ 0, & r > r_S, \end{cases} \tag{A2}$$

which gives relatively simple results. The quantized magnetic field is

$$\mathbf{B}(\mathbf{r},t) \equiv \mathbf{B}^{(+)}(\mathbf{r},t) + \mathbf{B}^{(-)}(\mathbf{r},t), \tag{A3}$$

where

$$\mathbf{B}^{(+)}(\mathbf{r},t) \equiv i\sum_{\mathbf{k},\alpha}\sqrt{\frac{\mu_0\hbar\omega_k}{2L^3}}\mathbf{f}_{\mathbf{k},\alpha}a_{\mathbf{k},\alpha}e^{i\mathbf{k}\cdot\mathbf{r}-i\omega_\mathbf{k}t}, \tag{A4}$$

$$\mathbf{B}^{(-)}(\mathbf{r},t) \equiv [\mathbf{B}^{(+)}(\mathbf{r},t)]^\dagger, \tag{A5}$$

$\omega_k = c|k|$, $\mathbf{f}_{\mathbf{k},\alpha}$ is a unit vector describing the polarization of mode $(\mathbf{k},\alpha)$ with annihilation operator $a_{\mathbf{k},\alpha}$, and L is the side length of the quantization volume, later taken to infinity. We similarly define $\bar{B}_z^{(+)}(t) \equiv \int d^3r\rho(\mathbf{r})\hat{z}\cdot\mathbf{B}^{(+)}(\mathbf{r},t)$ and $\bar{B}_z^{(-)}(t) \equiv [\bar{B}_z^{(+)}(t)]^\dagger$.

We can then use $\langle(aa^\dagger + a^\dagger a)/2\rangle = \langle a^\dagger a\rangle + 1/2 = \langle n\rangle + 1/2$, which for the thermal state of the field at temperature T_B has a value $1/2 + (\exp[\hbar\omega/k_BT_B] - 1) \approx 1/2 + k_BT_B/\hbar\omega$ when $k_BT_B \gg \hbar\omega$ (the Rayleigh-Jeans law), to obtain

$$\langle\bar{B}_z^2\rangle = \langle\bar{B}_z^{(-)}\bar{B}_z^{(+)} + \bar{B}_z^{(+)}\bar{B}_z^{(-)}\rangle \times\frac{\mu_0\hbar c}{L^3}\sum_{\mathbf{k},\alpha}\left(\frac{1}{2} + \frac{k_BT_B}{\hbar ck}\right)k|\mathbf{f}_{\mathbf{k},\alpha}\cdot\hat{z}|^2\left|\int d^3r\rho(\mathbf{r})e^{i\mathbf{k}\cdot\mathbf{r}}\right|^2. \tag{A6}$$

We compute the integral over $\mathbf{r}$ in spherical polar coordinates with the polar axis along $\mathbf{k}$:

$$\int d^3r\rho(\mathbf{r})e^{i\mathbf{k}\cdot\mathbf{r}} = \frac{2\pi}{V}\int_0^\pi \sin\theta_\rho d\theta_\rho\int_0^{r_S} r^2dre^{ikr\cos\theta_\rho} \times\frac{20\pi[(3-\zeta^2)\sin(\zeta) - 3\zeta\cos(\zeta)]}{k^3\zeta^2V}, \tag{A7}$$

where $\zeta \equiv kr_S$.

Now using spherical polar coordinates in which the polar axis is along $\hat{z}$, so that $\mathbf{k} = k(\sin\theta\cos\phi, \sin\theta\sin\phi, \cos\theta)$, and choosing polarization modes $\mathbf{f}_{\mathbf{k},\alpha}$ so that one is orthogonal to $\hat{z}$, the other has $\mathbf{f}_{\mathbf{k},\alpha}\cdot\hat{z} = \sin\theta$. Using the density of states $L^3/(2\pi)^3$, we have

$$\sum_{\mathbf{k},\alpha}|\mathbf{f}_{\mathbf{k},\alpha}\cdot\hat{z}|^2 \to \frac{L^3}{2^3\pi^3}\int k^2dk\sin^3\theta d\theta d\phi = \frac{L^3}{3\pi^2}\int k^2dk. \tag{A8}$$

Combining them, we find

$$\langle\bar{B}_z^2\rangle = \frac{\mu_0\hbar c}{L^3}\frac{L^3}{3\pi^2}\int_0^\infty dk\left(\frac{1}{2}k^3 + \frac{k_BT_B}{\hbar c}k^2\right) \times\left|\frac{20\pi[(3-\zeta^2)\sin(\zeta) - 3\zeta\cos(\zeta)]}{k^3\zeta^2V}\right|^2 \times\frac{25c\mu_0}{8\pi^2r_S^4}\hbar + \frac{5\mu_0}{7\pi r_S^3}k_BT_B. \tag{A9}$$

This gives the sensitivity of a single instantaneous measurement. To avoid measurement backaction it is necessary to wait a finite time before making the next measurement: The measurement will introduce noise into the observable conjugate to $\bar{B}_z(t)$, and by Maxwell's equations this disturbance will propagate into $\bar{B}_z(t' > t)$. The disturbance will propagate fully outside of $\mathcal{R}$ (it will always propagate at c) in a time $T_{\text{eff}} = 2r_S/c$, enabling backaction-free repeated measurements with repeat period T_{eff}.

The resulting energy resolution per bandwidth is

$$E_R = \frac{\langle\bar{B}_z^2\rangle VT_{\text{eff}}}{2\mu_0}\frac{175}{42\pi}\hbar + \frac{20r_S}{21c}k_BT_B. \tag{A10}$$

The first term describes the quantum noise contribution to the measurement. The prefactor (here $175/42\pi \approx 1.3$) depends on the precise choice of weighting function $\rho(\mathbf{r})$.

APPENDIX B: ZERO-POINT MAGNETIC NOISE AND SPIN-PRECESSION SENSORS

A paradigmatic field-sensing protocol with spin systems consists of preparing a magnetic spin system in a known direction, allowing it to interact with the field for a known free-precession time T, and detecting the spin orientation by a projective measurement. Here we consider the role of zero-point fluctuations of the field in this protocol.

We first consider this scenario semiclassically. It is sufficient to consider a Hilbert space $\mathcal{H} = \mathcal{H}_M$ describing the material system (here and afterward we use the subscripts $_M$ and $_F$ to indicate material and field, respectively) with dynamics governed by the Hamiltonian

$$H_{SC} = H_M + H_{MF}. \tag{B1}$$

Here the spin-field interaction is $H_{MF} = -\mu\cdot\mathbf{B} = -\gamma\hbar\mathbf{S}\cdot\mathbf{B}$, where $\mathbf{S}$ is the net spin and γ is the gyromagnetic ratio. In this semiclassical description, $\mathbf{B}$ is a c-number field and is unchanged by the interaction with the material system.

For the protocol to be efficient, it should be possible to prepare a stable, strongly polarized state of the material system, and this state should be free to rotate. We thus assume the following properties of H_M. (1) The ground state is continuously degenerate under rotations such that any state of the form $R_S(\mathbf{n},\theta)|\psi_0\rangle_M$ is a ground state, where $R_S(\mathbf{n},\theta)$ rotates all spins about an axis $\mathbf{n}$ by angle θ. (2) The reference ground state $|\psi_0\rangle_M$ is polarized: $S_z|\psi_0\rangle_M = S|\psi_0\rangle_M$. (3) The ground states are separated from any non-spin-S states by an energy gap. (4) For simplicity, we assume decoupling of spin

and center-of-mass degrees of freedom. Unlike a compass needle, here a spin rotation does not imply a rotation of the mass of the system. These assumptions describe an isotropic ferromagnet, but also a single electron, an atom with a non-spin-zero ground state, or a single-domain spinor condensate.

Starting from any ground state of this system, evolution under a small classical B field simply rotates within the space of ground states of H_{M}, with no addition of energy or entropy. The intrinsic angular noise in the sensing protocol is then independent of T, leading to a variance of the inferred field $\langle \delta B^2 \rangle \propto T^{-2}$ and $E_R \propto T^{-1} \to 0$ for large T.

To consider this protocol with a quantized field, we first expand the Hilbert space and Hamiltonian to include the field: $\mathcal{H}_{\mathrm{MF}} \equiv \mathcal{H}_{\mathrm{M}} \otimes \mathcal{H}_{\mathrm{F}}$ and

$$H = H_{\mathrm{M}} \otimes \mathbb{I}_{\mathrm{F}} + \mathbb{I}_{\mathrm{M}} \otimes H_{\mathrm{F}} + H_{\mathrm{MF}}. \tag{B2}$$

Here $H_{\mathrm{F}} = \int d^3x (\epsilon_0 \mathbf{E} \cdot \mathbf{E}/2 + \mathbf{B} \cdot \mathbf{B}/2\mu_0)$ is the field Hamiltonian. $\mathbb{I}_{\mathrm{M}}$ and $\mathbb{I}_{\mathrm{F}}$ indicate identity operators. $\mathbf{E}$ and $\mathbf{B}$ are quantized fields. The ground state of H_{F} is the vacuum state $|0\rangle_{\mathrm{F}}$.

For simplicity, we consider using the sensor to estimate an externally applied field that is constant in time and uniformly distributed, making a contribution $\bar{\mathbf{B}}$ (a c-number vector) to the value of the field $\mathbf{B}(\mathbf{x})$. Such a contribution is described by a displacement operator $D_{\bar{\mathbf{B}}}$, defined such that $D_{\bar{\mathbf{B}}}^{\dagger} \mathbf{B}(\mathbf{x}, t) D_{\bar{\mathbf{B}}} = \mathbf{B}(\mathbf{x}, t) + \bar{\mathbf{B}}$. We note that the remaining field $\tilde{\mathbf{B}}(\mathbf{x}, t) \equiv \mathbf{B}(\mathbf{x}) - \bar{\mathbf{B}}$ describes both the zero-point field fluctuations and any field produced by the sensor itself. We can consider the effect of this external field on the system as a whole by displacing the H of Eq. (B2) to find

$$D_{\bar{\mathbf{B}}}^{\dagger} H D_{\bar{\mathbf{B}}} = H_{\mathrm{M}} \otimes \mathbb{I}_{\mathrm{F}} + \mathbb{I}_{\mathrm{M}} \otimes H_{\mathrm{F}} + H_{\mathrm{MF}} + \frac{L^3}{2\mu_0} |\bar{\mathbf{B}}|^2 \mathbb{I}_{\mathrm{M}} \otimes \mathbb{I}_{\mathrm{F}} - \gamma \hbar \bar{\mathbf{B}} \cdot \mathbf{S} \otimes \mathbb{I}_{\mathrm{F}}, \tag{B3}$$

where L^3 is the volume of the calculation. The last two terms describe the classical energy of the external field $\bar{\mathbf{B}}$ and the interaction of the spin with the external field, respectively. This last contribution produces a torque $\gamma \mathbf{S} \times \bar{\mathbf{B}}$ on $\mathbf{S}$, and thereby induces a precession of $\mathbf{S}$ about $\bar{\mathbf{B}}$.

The dynamics of $\mathbf{S}$ in this fully quantized model will depend on what one takes to be the initial state. If one takes $|\psi_0\rangle_{\mathrm{M}} \otimes |0\rangle_{\mathrm{F}}$, i.e., a product of the material ground state and vacuum, the state will evolve, as it is not an eigenstate of H, which contains H_{MF}. Given the "white noise" character of vacuum fluctuations, it is not implausible that this evolution would produce a diffusion of $\mathbf{S}$, with an angular variance $\propto T$, a variance of the field estimate $\langle \delta B^2 \rangle \propto T^{-1}$, and thus $E_R \propto T^0$, which describes an ERL. An estimate of the limiting value of E_R is given in Sec. VI.C.

It is not clear that $|\psi_0\rangle_{\mathrm{M}} \otimes |0\rangle_{\mathrm{F}}$ is a realistic starting condition, however. It describes a scenario in which the spin $\mathbf{S}$ is oriented along a specific direction but the field around it is, on average, zero. It thus describes a condition in which the spin has not (or not yet) produced a dipolar field around itself. This "bare spin" condition is one that we do not expect to arise naturally in any experiment. And even if a bare spin could be made in some way, it surely would not remain bare for long.

A more reasonable starting condition is the "dressed" version of $|\psi_0\rangle_{\mathrm{M}}$, which is to say a ground state of H with the same symmetry under rotations as $|\psi_0\rangle_{\mathrm{M}} \otimes |0\rangle_{\mathrm{F}}$. In such a state, the field $\mathbf{B}(\mathbf{x})$ will presumably contain, in addition to vacuum fluctuations, the dipole field pattern produced by the magnetic moment μ. We note that H and its components are all invariant under rotations of the coordinate system or, equivalently, of $\mathbf{S}$, $\mathbf{B}(\mathbf{x})$, and $\mathbf{x}$ together. The ground state of H_{F} is irrotational or spin 0, and the ground state of H_{M} is (by assumption) of spin S. When these subsystems are perturbatively coupled by the irrotational H_{MF}, $|\psi_0\rangle_{\mathrm{M}} \otimes |0\rangle_{\mathrm{F}}$ becomes a dressed ground state $|\Psi_0\rangle_{\mathrm{MF}}$ with the same symmetry under global rotations.[2] In the same way, the other bare ground states $R_{\mathrm{S}}(\mathbf{n}, \theta)|\psi_0\rangle_{\mathrm{M}} \otimes |0\rangle_{\mathrm{F}}$ give rise to spin-rotated and field-rotated states $R_{\mathrm{S}}(\mathbf{n}, \theta) \otimes R_{\mathrm{F}}(\mathbf{n}, \theta)|\Psi_0\rangle_{\mathrm{MF}}$, where $R_{\mathrm{F}}(\mathbf{n}, \theta)$ is the field rotation operator. As ground states of the total Hamiltonian, they do not evolve in any way for $\bar{\mathbf{B}} = \mathbf{0}$, and the intrinsic spin uncertainty is independent of T.

We note that $|\Psi_0\rangle_{\mathrm{MF}}$ is an entangled state of the material and field, and that the field must carry some of the angular momentum. A projective measurement on the bare spin (if such a measurement could be made) would then have an additional intrinsic uncertainty, owing to the fact that the material spin system is one component of an entangled state. In contrast to the hypothetical diffusion of the spin orientation described previously, this would be a one-time noise contribution, in effect a contribution to the intrinsic spin noise of the state. Such a contribution would not change the scaling of E_R with T.

For an applied field $\bar{\mathbf{B}} \neq \mathbf{0}$, the torque on $\mathbf{S}$ will cause precession of the spin and a matched rotation of the field it generates via H_{MF}. In contrast to the semiclassical case, the system will not remain exactly within the manifold of dressed states. Rather, the precessing spin presents an oscillating magnetic dipole and will radiate, whereas the dressed ground states $R_{\mathrm{S}}(\mathbf{n}, \theta) \otimes R_{\mathrm{F}}(\mathbf{n}, \theta)|\Psi_0\rangle_{\mathrm{MF}}$ have no radiating component. Via radiation, the spin will lose energy and eventually align with or against $\bar{\mathbf{B}}$, depending on the sign of γ. The rate of radiative relaxation scales as $\bar{\mathbf{B}}^3$, so small fields could still be measured with very small E_R by the simple protocol considered thus far. We conclude that zero-point fluctuations do not in fact set a limit to E_R in a spin-precession measurement.

Finally, we note that an only slightly more complex protocol achieves $E_R \to 0$ also for strong fields. There will be some maximum degree of relaxation for which the state remains effectively within the dressed ground state manifold and the relaxation-free scaling $\langle \delta B^2 \rangle \propto T^{-2}$ holds. This implies a maximum free-precession time $\propto \bar{B}^{-3}$, where

[2]We assume here that a perturbative treatment is appropriate. A sufficiently strong coupling could, in principle, take the system through a quantum phase transition, with the result that the ground states of H have different symmetry than the ground states of $H_{\mathrm{M}} + H_{\mathrm{F}}$. This does not seem to be the case in quantum electrodynamics, in which dressed spins have the same symmetries as bare spins, and the coupling manifests in perturbative modifications to the spin properties, e.g., to the magnetic moments.

$\bar{B} = |\bar{\mathbf{B}}|$. A measurement made with this value of T has sensitivity $\langle \delta B^2 \rangle \propto \bar{B}^6$. Consider now a closed-loop measurement protocol in which $\bar{B} = B_{\text{unknown}} + B_{\text{control}}$, where B_{control} is a known control field and B_{unknown} is an unknown field to be estimated. The protocol uses a sequence of measurements of $\bar{B}$ and feedback to B_{control} to set $\bar{B}$ closer and closer to zero. The unknown field is inferred from the value of the control field that produces this condition.

Assuming the feedback procedure is limited by the intrinsic measurement variance $\langle \delta B^2 \rangle \propto \bar{B}^6$, then after the nth measurement, with variance $\langle \delta B^2 \rangle_n$, feedback achieves $\langle \bar{B} \rangle = 0$ and $\langle \delta \bar{B}^2 \rangle_n = \langle \delta B^2 \rangle_n$. If the free-precession time for the next measurement is then chosen $T_{n+1} \propto \langle \delta \bar{B}^2 \rangle_n^{-3/2}$ to ensure small relaxation, we find $T_{n+1} \propto T_n^3$ and thus $\langle \delta \bar{B}^2 \rangle_{n+1} \propto \langle \delta \bar{B}^2 \rangle_n^3$. Assuming that the first measurement could be made with sufficient precision to reduce the variance through the feeedback process, $\langle \delta \bar{B}^2 \rangle_n$ thus decreases very rapidly with n. The total time used in the protocol is dominated by the last measurement, and $E_R \to 0$.

REFERENCES

Acosta, V. M., D. Budker, P. R. Hemmer, J. R. Maze, and R. L. Walsworth, 2013, "Optical magnetometry with nitrogen-vacancy centers in diamond" in *Optical Magnetometry*, edited by D. Budker and D. F. Jackson Kimball (Cambridge University Press, Cambridge, England), pp. 142–166.

Aharonov, Y., and D. Bohm, 1961, "Time in the quantum theory and the uncertainty relation for time and energy," Phys. Rev. **122**, 1649.

Aharonov, Y., S. Massar, and S. Popescu, 2002, "Measuring energy, estimating Hamiltonians, and the time-energy uncertainty relation," Phys. Rev. A **66**, 052107.

Ahmadi, S., H. A. R. El-Ella, J. O. B. Hansen, A. Huck, and U. L. Andersen, 2017, "Pump-Enhanced Continuous-Wave Magnetometry Using Nitrogen-Vacancy Ensembles," Phys. Rev. Applied **8**, 034001.

Allred, J. C., R. N. Lyman, T. W. Kornack, and M. V. Romalis, 2002, "High-Sensitivity Atomic Magnetometer Unaffected by Spin-Exchange Relaxation," Phys. Rev. Lett. **89**, 130801.

Ariyaratne, A., D. Bluvstein, B. A. Myers, and A. C. B. Jayich, 2018, "Nanoscale electrical conductivity imaging using a nitrogen-vacancy center in diamond,"Nat. Commun. **9**, 2406.

Arridge, C., *et al.*, 2016, "Cassini *in situ* observations of long-duration magnetic reconnection in Saturn's magnetotail," Nat. Phys. **12**, 268.

Astner, T., *et al.*, 2018, "Solid-state electron spin lifetime limited by phononic vacuum modes," Nat. Mater. **17**, 313.

Awschalom, D. D., J. R. Rozen, M. B. Ketchen, W. J. Gallagher, A. W. Kleinsasser, R. L. Sandstrom, and B. Bumble, 1988, "Low-noise modular microsusceptometer using nearly quantum limited dc SQUIDs," Appl. Phys. Lett. **53**, 2108.

Bal, M., C. Deng, J.-L. Orgiazzi, F. R. Ong, and A. Lupascu, 2012, "Ultrasensitive magnetic field detection using a single artificial atom," Nat. Commun. **3**, 1324.

Balasubramanian, G., *et al.*, 2009, "Ultralong spin coherence time in isotopically engineered diamond," Nat. Mater. **8**, 383.

Band, Y. B., Y. Avishai, and A. Shnirman, 2018, "Dynamics of a Magnetic Needle Magnetometer: Sensitivity to Landau-Lifshitz-Gilbert Damping," Phys. Rev. Lett. **121**, 160801.

Barry, J. F., M. J. Turner, J. M. Schloss, D. R. Glenn, Y. Song, M. D. Lukin, H. Park, and R. L. Walsworth, 2016, "Optical magnetic detection of single-neuron action potentials using quantum defects in diamond," Proc. Natl. Acad. Sci. U.S.A. **113**, 14133.

Baumgart, I., J.-M. Cai, A. Retzker, M. B. Plenio, and C. Wunderlich, 2016, "Ultrasensitive Magnetometer Using a Single Atom," Phys. Rev. Lett. **116**, 240801.

Behbood, N., F. M. Ciurana, G. Colangelo, M. Napolitano, M. W. Mitchell, and R. J. Sewell, 2013, "Real-time vector field tracking with a cold-atom magnetometer," Appl. Phys. Lett. **102**, 173504.

Bekenstein, J. D., 1981a, "Energy Cost of Information Transfer," Phys. Rev. Lett. **46**, 623.

Bekenstein, J. D., 1981b, "Universal upper bound on the entropy-to-energy ratio for bounded systems," Phys. Rev. D **23**, 287.

Bekenstein, J. D., 1984, "Entropy content and information flow in systems with limited energy," Phys. Rev. D **30**, 1669.

Ben 'Attar, K. I. O., D. Farfurnik, and N. Bar-Gill, 2019, "Hamiltonian engineering of general two-body spin-1/2 interactions," arXiv:1906.00403.

Bending, S., 1999, "Local magnetic probes of superconductors," Adv. Phys. **48**, 449.

Berry-Pusey, B. N., B. C. Anger, G. Laicher, and B. Saam, 2006, "Nuclear spin relaxation of ^{129}Xe due to persistent xenon dimers," Phys. Rev. A **74**, 063408.

Boto, E., *et al.*, 2017, "A new generation of magnetoencephalography: Room temperature measurements using optically-pumped magnetometers," NeuroImage **149**, 404.

Brandt, E. H., and G. P. Mikitik, 2000, "Meissner-London Currents in Superconductors with Rectangular Cross Section," Phys. Rev. Lett. **85**, 4164.

Braun, D., G. Adesso, F. Benatti, R. Floreanini, U. Marzolino, M. W. Mitchell, and S. Pirandola, 2018, "Quantum-enhanced measurements without entanglement," Rev. Mod. Phys. **90**, 035006.

Braunstein, S. L., and C. M. Caves, 1994, "Statistical Distance and the Geometry of Quantum States," Phys. Rev. Lett. **72**, 3439.

Bremermann, H. J., 1982, "Minimum energy requirements of information transfer and computing," Int. J. Theor. Phys. **21**, 203.

Breuer, H., and F. Petruccione, 2007, *The Theory of Open Quantum Systems* (Oxford University Press, New York).

Budker, D., and M. Romalis, 2007, "Optical magnetometry," Nat. Phys. **3**, 227.

Caves, C. M., 1982, "Quantum limits on noise in linear amplifiers," Phys. Rev. D **26**, 1817.

Chann, B., I. A. Nelson, L. W. Anderson, B. Driehuys, and T. G. Walker, 2002, "^{129}Xe-Xe Molecular Spin Relaxation," Phys. Rev. Lett. **88**, 113201.

Chenaud, B., A. Segovia-Mera, A. Delgard, N. Feltin, A. Hoffmann, F. Pascal, W. Zawadzki, D. Mailly, and C. Chaubet, 2016, "Sensitivity and noise of micro-Hall magnetic sensors based on InGaAs quantum wells," J. Appl. Phys. **119**, 024501.

Choi, J., H. Zhou, H. S. Knowles, R. Landig, S. Choi, and M. D. Lukin, 2019, "Robust dynamic Hamiltonian engineering of many-body spin systems," arXiv:1907.03771.

Choi, S., N. Y. Yao, and M. D. Lukin, 2017, "Dynamical Engineering of Interactions in Qudit Ensembles," Phys. Rev. Lett. **119**, 183603.

Clevenson, H., M. E. Trusheim, C. Teale, T. Schroder, D. Braje, and D. Englund, 2015, "Broadband magnetometry and temperature sensing with a light-trapping diamond waveguide," Nat. Phys. **11**, 393.

Crepaz, H., L. Y. Ley, and R. Dumke, 2015, "Cavity enhanced atomic magnetometry," Sci. Rep. **5**, 15448.

Cromar, M., and P. Carelli, 1981, "Low-noise tunnel junction dc SQUID's," Appl. Phys. Lett. **38**, 723.

Dang, H. B., A. C. Maloof, and M. V. Romalis, 2010, "Ultrahigh sensitivity magnetic field and magnetization measurements with an atomic magnetometer," Appl. Phys. Lett. **97**, 151110.

Danilin, S., A. V. Lebedev, A. Vepsäläinen, G. B. Lesovik, G. Blatter, and G. S. Paraoanu, 2018, "Quantum-enhanced magnetometry by phase estimation algorithms with a single artificial atom," npj Quantum Inf. **4**, 29.

Davies, E., 1976, *Quantum Theory of Open Systems* (Academic Press, New York).

Dietsche, E. K., A. Larrouy, S. Haroche, J. M. Raimond, M. Brune, and S. Gleyzes, 2019, "High-sensitivity magnetometry with a single atom in a superposition of two circular Rydberg states," Nat. Phys. **15**, 326.

Doherty, M. W., N. B. Manson, P. Delaney, F. Jelezko, J. Wrachtrup, and L. C. L. Hollenberg, 2013, "The nitrogen-vacancy colour centre in diamond," Phys. Rep. **528**, 1.

Drung, D., S. Knappe, and H. Koch, 1995, "Theory for the multiloop dc superconducting quantum interference device magnetometer and experimental verification," J. Appl. Phys. **77**, 4088.

Eto, Y., H. Ikeda, H. Suzuki, S. Hasegawa, Y. Tomiyama, S. Sekine, M. Sadgrove, and T. Hirano, 2013, "Spin-echo-based magnetometry with spinor Bose-Einstein condensates," Phys. Rev. A **88**, 031602.

Faley, M. I., C. L. Jia, L. Houben, D. Meertens, U. Poppe, and K. Urban, 2006, "Meandering of the grain boundary and *d*-wave effects in high-T_c bicrystal Josephson junctions," Supercond. Sci. Technol. **19**, S195.

Faley, M. I., *et al.*, 2012, "Magnetoencephalography using a multilayer hight$_c$ DC SQUID magnetometer," Phys. Procedia **36**, 66.

Faley, M. I., *et al.*, 2013, "High-T_c DC SQUIDs for magnetoencephalography," IEEE Trans. Appl. Supercond. **23**, 1600705.

Fang, K., V. M. Acosta, C. Santori, Z. Huang, K. M. Itoh, H. Watanabe, S. Shikata, and R. G. Beausoleil, 2013, "High-Sensitivity Magnetometry Based on Quantum Beats in Diamond Nitrogen-Vacancy Centers," Phys. Rev. Lett. **110**, 130802.

Fescenko, I., A. Jarmola, I. Savukov, P. Kehayias, J. Smits, J. Damron, N. Ristoff, N. Mosavian, and V. M. Acosta, 2019, "Diamond magnetometer enhanced by ferrite flux concentrators," arXiv:1911.05070.

Fong, L. E., J. R. Holzer, K. K. McBride, E. A. Lima, F. Baudenbacher, and M. Radparvar, 2005, "High-resolution room-temperature sample scanning superconducting quantum interference device microscope configurable for geological and biomagnetic applications," Rev. Sci. Instrum. **76**, 053703.

Forstner, S., E. Sheridan, J. Knittel, C. L. Humphreys, G. A. Brawley, H. Rubinsztein-Dunlop, and W. P. Bowen, 2014, "Ultrasensitive optomechanical magnetometry," Adv. Mater. **26**, 6348.

Gallop, J., P. W. Josephs-Franks, J. Davies, L. Hao, and J. Macfarlane, 2002, "Miniature dc SQUID devices for the detection of single atomic spin-flips," Physica (Amsterdam) **368C**, 109.

Gawlik, W., and S. Pustelny, 2017, "Nonlinear magneto-optical rotation magnetometers," in *High Sensitivity Magnetometers*, edited by A. Grosz, M. J. Haji-Sheikh, and S. C. Mukhopadhyay (Springer International Publishing, Cham, Switzerland), pp. 425–450.

Gentile, T. R., P. J. Nacher, B. Saam, and T. G. Walker, 2017, "Optically polarized ^{3}He," Rev. Mod. Phys. **89**, 045004.

Giazotto, F., J. T. Peltonen, M. Meschke, and J. P. Pekola, 2010, "Superconducting quantum interference proximity transistor," Nat. Phys. **6**, 254.

Giovannetti, V., S. Lloyd, and L. Maccone, 2004, "Quantum-enhanced measurements: Beating the standard quantum limit," Science **306**, 1330.

Giovannetti, V., S. Lloyd, and L. Maccone, 2006, "Quantum Metrology," Phys. Rev. Lett. **96**, 010401.

Griffith, W. C., S. Knappe, and J. Kitching, 2010, "Femtotesla atomic magnetometry in a microfabricated vapor cell," Opt. Express **18**, 27167.

Griffiths, D. J., 1999, *Introduction to Electrodynamics*, 3rd ed. (Benjamin Cummings, San Francisco).

Grosz, A., M. Haji-Sheikh, and S. Mukhopadhyay, 2016, *High Sensitivity Magnetometers*, Smart Sensors, Measurement and Instrumentation Vol. 19 (Springer, New York).

Haas, H., D. Puzzuoli, F. Zhang, and D. G. Cory, 2019, "Engineering effective Hamiltonians," arXiv:1904.02702.

Hankard, F., J. Gattacceca, C. Fermon, M. Pannetier-Lecoeur, B. Langlais, Y. Quesnel, P. Rochette, and S. A. McEnroe, 2009, "Magnetic field microscopy of rock samples using a giant magnetoresistance–based scanning magnetometer," Geochem. Geophys. Geosyst. **10**, Q10Y06.

Helstrom, C. W., 1969, "Quantum detection and estimation theory," J. Stat. Phys. **1**, 231.

Helstrom, C. W., 1976, *Quantum Detection and Estimation Theory* (Academic Press, New York).

Higbie, J. M., L. E. Sadler, S. Inouye, A. P. Chikkatur, S. R. Leslie, K. L. Moore, V. Savalli, and D. M. Stamper-Kurn, 2005, "Direct Nondestructive Imaging of Magnetization in a Spin-1 Bose-Einstein Gas," Phys. Rev. Lett. **95**, 050401.

Hite, D., Y. Colombe, A. Wilson, D. Allcock, D. Leibfried, D. Wineland, and D. Pappas, 2013, "Surface science for improved ion traps," MRS Bull. **38**, 826.

Huang, L., Z. Zhang, B. Chen, X. Ma, H. Zhong, and L.-M. Peng, 2014, "Ultra-sensitive graphene Hall elements," Appl. Phys. Lett. **104**, 183106.

Ingarden, R., A. Kossakowski, and M. Ohya, 1997, *Information Dynamics and Open Systems: Classical and Quantum Approach*, Fundamental Theories of Physics (Springer, New York).

Jackson Kimball, D. F., A. O. Sushkov, and D. Budker, 2016, "Precessing Ferromagnetic Needle Magnetometer," Phys. Rev. Lett. **116**, 190801.

Jasperse, M., M. J. Kewming, S. N. Fischer, P. Pakkiam, R. P. Anderson, and L. D. Turner, 2017, "Continuous Faraday measurement of spin precession without light shifts," Phys. Rev. A **96**, 063402.

Jeng, J., J. Chen, and C. Lu, 2012, "Enhancement in sensitivity using multiple harmonics for miniature fluxgates," IEEE Trans. Magn. **48**, 3696.

Jensen, K., P. Kehayias, and D. Budker, 2017, "Magnetometry with nitrogen-vacancy centers in diamond," in *High Sensitivity Magnetometers*, edited by A. Grosz, M. J. Haji-Sheikh, and S. C. Mukhopadhyay (Springer International Publishing, Cham, Switzerland), pp. 553–576.

Jiménez-Martínez, R., and S. Knappe, 2017, "Microfabricated optically-pumped magnetometers," in *High Sensitivity Magnetometers*, edited by A. Grosz, M. J. Haji-Sheikh, and S. C. Mukhopadhyay (Springer International Publishing, Cham, Switzerland), pp. 523–551.

Kadlecek, S., T. Walker, D. K. Walter, C. Erickson, and W. Happer, 2001, "Spin-axis relaxation in spin-exchange collisions of alkali-metal atoms," Phys. Rev. A **63**, 052717.

Kawai, J., H. Oda, J. Fujihira, M. Miyamoto, I. Miyagi, and M. Sato, 2016, "SQUID microscope with hollow-structured cryostat for magnetic field imaging of room temperature samples," IEEE Trans. Appl. Supercond. **26**, 1.

Kher, A., P. Day, B. H. Eom, H. Leduc, and J. Zmuidzinas, 2013, "Superconducting nonlinear kinetic inductance devices"

(unpublished), http://www.eucas2013.spin.cnr.it/sites/default/files/scientific_program.pdf.

Kher, A., P. K. Day, B. H. Eom, J. Zmuidzinas, and H. G. Leduc, 2016, "Kinetic inductance parametric up-converter," J. Low Temp. Phys. **184**, 480.

Kher, A. S., 2017, "Superconducting nonlinear kinetic inductance devices," Ph.D. thesis (California Institute of Technology).

Kim, Y. J., and I. Savukov, 2016, "Ultra-sensitive magnetic microscopy with an optically pumped magnetometer," Sci. Rep. **6**, 24773.

Kirtley, J. R., 2010, "Fundamental studies of superconductors using scanning magnetic imaging," Rep. Prog. Phys. **73**, 126501.

Kirtley, J. R., *et al.*, 2016, "Scanning SQUID susceptometers with sub-micron spatial resolution," Rev. Sci. Instrum. **87**, 093702.

Kitching, J., 2012 (private communication).

Koch, R. H., D. J. Van Harlingen, and J. Clarke, 1980, "Quantum-Noise Theory for the Resistively Shunted Josephson Junction," Phys. Rev. Lett. **45**, 2132.

Koch, R. H., D. J. Van Harlingen, and J. Clarke, 1981, "Quantum noise theory for the dc SQUID," Appl. Phys. Lett. **38**, 380.

Kominis, I., T. Kornack, J. Allred, and M. Romalis, 2003, "A subfemtotesla multichannel atomic magnetometer," Nature (London) **422**, 596.

Krey, S., H. J. Barthelmess, and M. Schilling, 1999, "Low-frequency noise and linearity of a $YBa_2Cu_3O_7$ dc superconducting quantum interference device magnetometer in static magnetic fields," J. Appl. Phys. **86**, 6602.

Ledbetter, M. P., I. M. Savukov, V. M. Acosta, D. Budker, and M. V. Romalis, 2008, "Spin-exchange-relaxation-free magnetometry with Cs vapor," Phys. Rev. A **77**, 033408.

Lee, H., P. Kok, and J. P. Dowling, 2002, "A quantum Rosetta stone for interferometry," J. Mod. Opt. **49**, 2325.

Lee, S.-K., 2019 "Linear amplifier noise relation satisfied by an atomic magnetometer (revised)" (private communication).

Lee, S.-K., and M. V. Romalis, 2008, "Back-reaction and dipolar interaction noise of a spin magnetometer," in *Proceedings of the 39th Annual Meeting of the APS Division of Atomic, Molecular, and Optical Physics, State College, PA, 2008*, http://meetings.aps.org/link/BAPS.2008.DAMOP.R1.123.

Lima, E. A., A. C. Bruno, H. R. Carvalho, and B. P. Weiss, 2014, "Scanning magnetic tunnel junction microscope for high-resolution imaging of remanent magnetization fields," Meas. Sci. Technol. **25**, 105401.

Lindblad, C., 2001, *Non-Equilibrium Entropy and Irreversibility*, Mathematical Physics Studies (Springer, Dordrecht).

Lovchinsky, I., *et al.*, 2016, "Nuclear magnetic resonance detection and spectroscopy of single proteins using quantum logic," Science **351**, 836.

Luomahaara, J., V. Vesterinen, L. Grönberg, and J. Hassel, 2014, "Kinetic inductance magnetometer," Nat. Commun. **5**, 4872.

Maletinsky, P., S. Hong, M. S. Grinolds, B. Hausmann, M. D. Lukin, R. L. Walsworth, M. Loncar, and A. Yacoby, 2012, "A robust scanning diamond sensor for nanoscale imaging with single nitrogen-vacancy centres," Nat. Nanotechnol. **7**, 320.

Marauska, S., R. Jahns, C. Kirchhof, M. Claus, E. Quandt, R. Knöchel, and B. Wagner, 2013, "Highly sensitive wafer-level packaged MEMS magnetic field sensor based on magnetoelectric composites," Sens. Actuators A **189**, 321.

Margolus, N., and L. B. Levitin, 1998, "The maximum speed of dynamical evolution," Physica (Amsterdam) **120D**, 188.

Mitchell, M. W., 2017, "Number-unconstrained quantum sensing," Quantum Sci. Technol. **2**, 044005.

Mitchell, M. W., 2020, "Scale-invariant spin dynamics and the quantum limits of field sensing," New J. Phys. (to be published), https://doi.org/10.1088/1367-2630/ab81b8.

Mück, M., J. B. Kycia, and J. Clarke, 2001, "Superconducting quantum interference device as a near-quantum-limited amplifier at 0.5 Ghz," Appl. Phys. Lett. **78**, 967.

Muessel, W., H. Strobel, D. Linnemann, D. B. Hume, and M. K. Oberthaler, 2014, "Scalable Spin Squeezing for Quantum-Enhanced Magnetometry with Bose-Einstein Condensates," Phys. Rev. Lett. **113**, 103004.

Myers, B. A., A. Ariyaratne, and A. C. B. Jayich, 2017, "Double-Quantum Spin-Relaxation Limits to Coherence of Near-Surface Nitrogen-Vacancy Centers," Phys. Rev. Lett. **118**, 197201.

Newbury, N. R., A. S. Barton, G. D. Cates, W. Happer, and H. Middleton, 1993, "Gaseous ^{3}-^{3}He magnetic dipolar spin relaxation," Phys. Rev. A **48**, 4411.

Ockeloen, C. F., R. Schmied, M. F. Riedel, and P. Treutlein, 2013, "Quantum Metrology with a Scanning Probe Atom Interferometer," Phys. Rev. Lett. **111**, 143001.

Oda, H., *et al.*, 2016, "Scanning SQUID microscope system for geological samples: System integration and initial evaluation," Earth Planets Space **68**, 179.

Oral, A., M. Kaval, M. Dede, H. Masuda, A. Okamoto, I. Shibasaki, and A. Sandhu, 2002, "Room-temperature scanning hall probe microscope (RT-SHPM) imaging of garnet films using new high-performance InSb sensors," IEEE Trans. Magn. **38**, 2438.

Palacios, S., S. Coop, P. Gomez, T. Vanderbruggen, Y. N. M. de Escobar, M. Jasperse, and M. W. Mitchell, 2018, "Multi-second magnetic coherence in a single domain spinor Bose–Einstein condensate," New J. Phys. **20**, 053008.

Pannetier, M., C. Fermon, G. Le Goff, J. Simola, and E. Kerr, 2004, "Femtotesla magnetic field measurement with magnetoresistive sensors," Science **304**, 1648.

Pezzè, L., A. Smerzi, M. K. Oberthaler, R. Schmied, and P. Treutlein, 2018, "Quantum metrology with nonclassical states of atomic ensembles," Rev. Mod. Phys. **90**, 035005.

Pham, L. M., N. Bar-Gill, C. Belthangady, D. Le Sage, P. Cappellaro, M. D. Lukin, A. Yacoby, and R. L. Walsworth, 2012, "Enhanced solid-state multispin metrology using dynamical decoupling," Phys. Rev. B **86**, 045214.

Riek, C., D. V. Seletskiy, A. S. Moskalenko, J. F. Schmidt, P. Krauspe, S. Eckart, S. Eggert, G. Burkard, and A. Leitenstorfer, 2015, "Direct sampling of electric-field vacuum fluctuations," Science **350**, 420.

Robbes, D., 2006, "Highly sensitive magnetometers—A review," Sens. Actuators A **129**, 86.

Romalis, M. V., D. Sheng, B. Saam, and T. G. Walker, 2014, "Comment on 'New Limit on Lorentz-Invariance- and *cpt*-Violating Neutron Spin Interactions Using a Free-Spin-Precession ^{3}He – ^{129}Xe Comagnetometer,'" Phys. Rev. Lett. **113**, 188901.

Rondin, L., J.-P. Tetienne, T. Hingant, J.-F. Roch, P. Maletinsky, and V. Jacques, 2014, "Magnetometry with nitrogen-vacancy defects in diamond," Rep. Prog. Phys. **77**, 056503.

Rotter, I., and J. P. Bird, 2015, "A review of progress in the physics of open quantum systems: Theory and experiment," Rep. Prog. Phys. **78**, 114001.

Roy, S. M., and S. L. Braunstein, 2008, "Exponentially Enhanced Quantum Metrology," Phys. Rev. Lett. **100**, 220501.

Ruster, T., H. Kaufmann, M. A. Luda, V. Kaushal, C. T. Schmiegelow, F. Schmidt-Kaler, and U. G. Poschinger, 2017, "Entanglement-Based dc Magnetometry with Separated Ions," Phys. Rev. X **7**, 031050.

Ryhänen, T., H. Seppä, R. Ilmoniemi, and J. Knuutila, 1989, "SQUID magnetometers for low-frequency applications," J. Low Temp. Phys. **76**, 287.

Savukov, I. M., 2017, "Spin exchange relaxation free (SERF) magnetometers," in *High Sensitivity Magnetometers*, edited by A. Grosz, M. J. Haji-Sheikh, and S. C. Mukhopadhyay (Springer International Publishing, Cham, Switzerland), pp. 451–491.

Savukov, I. M., S. J. Seltzer, M. V. Romalis, and K. L. Sauer, 2005, "Tunable Atomic Magnetometer for Detection of Radio-Frequency Magnetic Fields," Phys. Rev. Lett. **95**, 063004.

Schiffer, M., 1991, "Quantum limit for information transmission," Phys. Rev. A **43**, 5337.

Schmelz, M., R. Stolz, V. Zakosarenko, T. Schönau, S. Anders, L. Fritzsch, M. Mück, and H.-G. Meyer, 2011, "Field-stable SQUID magnetometer with sub-fT $Hz^{-1/2}$ resolution based on sub-micrometer cross-type Josephson tunnel junctions," Supercond. Sci. Technol. **24**, 065009.

Schmelz, M., V. Zakosarenko, A. Chwala, T. Schönau, R. Stolz, S. Anders, S. Linzen, and H. Meyer, 2016, "Thin-film-based ultralow noise SQUID magnetometer," IEEE Trans. Appl. Supercond. **26**, 1.

Schmelz, M., V. Zakosarenko, T. Schönau, S. Anders, S. Linzen, R. Stolz, and H.-G. Meyer, 2017, "Nearly quantum limited nano-SQUIDs based on cross-type $Nb/Alo_x/Nb$ junctions," Supercond. Sci. Technol. **30**, 014001.

Schmied, R., J.-D. Bancal, B. Allard, M. Fadel, V. Scarani, P. Treutlein, and N. Sangouard, 2016, "Bell correlations in a Bose-Einstein condensate," Science **352**, 441.

Schwindt, P. D. D., S. Knappe, V. Shah, L. Hollberg, J. Kitching, L.-A. Liew, and J. Moreland, 2004, "Chip-scale atomic magnetometer," Appl. Phys. Lett. **85**, 6409.

Schwindt, P. D. D., B. Lindseth, S. Knappe, V. Shah, J. Kitching, and L.-A. Liew, 2007, "Chip-scale atomic magnetometer with improved sensitivity by use of the Mx technique," Appl. Phys. Lett. **90**, 081102.

Sewell, R. J., M. Koschorreck, M. Napolitano, B. Dubost, N. Behbood, and M. W. Mitchell, 2012, "Magnetic Sensitivity Beyond the Projection Noise Limit by Spin Squeezing," Phys. Rev. Lett. **109**, 253605.

Shah, V., S. Knappe, P. D. D. Schwindt, and J. Kitching, 2007, "Subpicotesla atomic magnetometry with a microfabricated vapour cell," Nat. Photonics **1**, 649.

Sheng, D., S. Li, N. Dural, and M. V. Romalis, 2013, "Subfemtotesla Scalar Atomic Magnetometry Using Multipass Cells," Phys. Rev. Lett. **110**, 160802.

Smullin, S. J., I. M. Savukov, G. Vasilakis, R. K. Ghosh, and M. V. Romalis, 2009, "Low-noise high-density alkali-metal scalar magnetometer," Phys. Rev. A **80**, 033420.

Sørensen, A. S., and K. Mølmer, 2001, "Entanglement and Extreme Spin Squeezing," Phys. Rev. Lett. **86**, 4431.

Storm, J.-H., P. Hömmen, D. Drung, and R. Körber, 2017, "An ultra-sensitive and wideband magnetometer based on a superconducting quantum interference device," Appl. Phys. Lett. **110**, 072603.

Taylor, J. M., P. Cappellaro, L. Childress, L. Jiang, D. Budker, P. R. Hemmer, A. Yacoby, R. Walsworth, and M. D. Lukin, 2008, "High-sensitivity diamond magnetometer with nanoscale resolution," Nat. Phys. **4**, 810.

Tesche, C. D., and J. Clarke, 1977, "dc SQUID: Noise and optimization," J. Low Temp. Phys. **29**, 301.

Tighineanu, P., M. L. Andersen, A. S. Sørensen, S. Stobbe, and P. Lodahl, 2014, "Probing Electric and Magnetic Vacuum Fluctuations with Quantum Dots," Phys. Rev. Lett. **113**, 043601.

Trusheim, M. E., L. Li, A. Laraoui, E. H. Chen, H. Bakhru, T. Schröder, O. Gaathon, C. A. Meriles, and D. Englund, 2014, "Scalable fabrication of high purity diamond nanocrystals with long-spin-coherence nitrogen vacancy centers," Nano Lett. **14**, 32.

Tura, J., R. Augusiak, A. B. Sainz, T. Vértesi, M. Lewenstein, and A. Acín, 2014, "Detecting nonlocality in many-body quantum states," Science **344**, 1256.

Van Harlingen, D. J., R. H. Koch, and J. Clarke, 1982, "Superconducting quantum interference device with very low magnetic flux noise energy," Appl. Phys. Lett. **41**, 197.

Vasyukov, D., *et al.*, 2013, "A scanning superconducting quantum interference device with single electron spin sensitivity," Nat. Nanotechnol. **8**, 639.

Vengalattore, M., J. M. Higbie, S. R. Leslie, J. Guzman, L. E. Sadler, and D. M. Stamper-Kurn, 2007, "High-Resolution Magnetometry with a Spinor Bose-Einstein Condensate," Phys. Rev. Lett. **98**, 200801.

Vetoshko, P. M., M. V. Valeiko, and P. I. Nikitin, 2003, "Epitaxial yttrium iron garnet film as an active medium of an even-harmonic magnetic field transducer," Sens. Actuators A **106**, 270.

Vinante, A., P. Falferi, G. Gasbarri, A. Setter, C. Timberlake, and H. Ulbricht, 2019, "Ultrahigh mechanical quality factor with Meissner-levitated ferromagnetic microparticles," arXiv:1912.12252.

Viola, L., and S. Lloyd, 1998, "Dynamical suppression of decoherence in two-state quantum systems," Phys. Rev. A **58**, 2733.

Wakai, R. T., and D. J. Van Harlingen, 1988, "Signal and white noise properties of edge junction dc SQUID's," Appl. Phys. Lett. **52**, 1182.

Wald, R. M., 1979, "Entropy and black-hole thermodynamics," Phys. Rev. D **20**, 1271.

Wang, Y., J. Gao, M. Li, D. Hasanyan, Y. Shen, J. Li, D. Viehland, and H. Luo, 2012, "Ultralow equivalent magnetic noise in a magnetoelectric Metglas/Mn-doped Pb $(Mg_{1/3}Nb_{2/3})O_3$-$PbTiO_3$ heterostructure," Appl. Phys. Lett. **101**, 022903.

Weis, A., G. Bison, and Z. D. Grujić, 2017, "Magnetic resonance based atomic magnetometers," in *High Sensitivity Magnetometers*, edited by A. Grosz, M. J. Haji-Sheikh, and S. C. Mukhopadhyay (Springer International Publishing, Cham, Switzerland), pp. 361–424.

Wildermuth, S., S. Hofferberth, I. Lesanovsky, S. Groth, P. Krüger, J. Schmiedmayer, and I. Bar-Joseph, 2006, "Sensing electric and magnetic fields with Bose-Einstein condensates," Appl. Phys. Lett. **88**, 264103.

Wildermuth, S., S. Hofferberth, I. Lesanovsky, E. Haller, L. Andersson, S. Groth, I. Bar-Joseph, P. Krüger, and J. Schmiedmayer, 2005, "Bose-Einstein condensates: Microscopic magnetic-field imaging," Nature (London) **435**, 440.

Wildermuth, S., P. Krüger, C. Becker, M. Brajdic, S. Haupt, A. Kasper, R. Folman, and J. Schmiedmayer, 2004, "Optimized magneto-optical trap for experiments with ultracold atoms near surfaces," Phys. Rev. A **69**, 030901.

Wolf, T., P. Neumann, K. Nakamura, H. Sumiya, T. Ohshima, J. Isoya, and J. Wrachtrup, 2015, "Subpicotesla Diamond Magnetometry," Phys. Rev. X **5**, 041001.

Wood, A. A., L. M. Bennie, A. Duong, M. Jasperse, L. D. Turner, and R. P. Anderson, 2015, "Magnetic tensor gradiometry using Ramsey interferometry of spinor condensates," Phys. Rev. A **92**, 053604.

Yang, F., A. J. Kollár, S. F. Taylor, R. W. Turner, and B. L. Lev, 2017, "Scanning Quantum Cryogenic Atom Microscope," Phys. Rev. Applied **7**, 034026.

Zhou, H., *et al.*, 2019, "Quantum metrology with strongly interacting spin systems," arXiv:1907.10066.